Contributions of climate feedbacks to changes in atmospheric circulation

Article

Published Version

It is advisable to refer to the publisher's version if you intend to cite from the work. See Guidance on citing.
Published version at: https://doi.org/10.1175/JCLI-D-17-0189.1
To link to this article DOI: http://dx.doi.org/10.1175/JCLI-D-17-0189.1

Publisher: American Meteorological Society

www.reading.ac.uk/centaur

CentAUR

Central Archive at the University of Reading

Contributions of Climate Feedbacks to Changes in Atmospheric Circulation

Paulo Ceppi and Theodore G. Shepherd

Department of Meteorology, University of Reading, Reading, United Kingdom

ABSTRACT

The projected response of the atmospheric circulation to the radiative changes induced by CO_2 forcing and climate feedbacks is currently uncertain. In this modeling study, the impact of CO_2-induced climate feedbacks on changes in jet latitude and speed is assessed by imposing surface albedo, cloud, and water vapor feedbacks as if they were forcings in two climate models, CAM4 and ECHAM6. The jet response to radiative feedbacks can be broadly interpreted through changes in midlatitude baroclinicity. Clouds enhance baroclinicity, favoring a strengthened, poleward-shifted jet; this is mitigated by surface albedo changes, which have the opposite effect on baroclinicity and the jet, while water vapor has opposing effects on upper- and lower-level baroclinicity with little net impact on the jet. Large differences between the CAM4 and ECHAM6 responses illustrate how model uncertainty in radiative feedbacks causes a large spread in the baroclinicity response to CO_2 forcing. Across the CMIP5 models, differences in shortwave feedbacks by clouds and albedo are a dominant contribution to this spread. Forcing CAM4 with shortwave cloud and albedo feedbacks from a representative set of CMIP5 models yields a wide range of jet responses that strongly correlate with the meridional gradient of the anomalous shortwave heating and the associated baroclinicity response. Differences in shortwave feedbacks statistically explain about 50% of the intermodel spread in CMIP5 jet shifts for the set of models used, demonstrating the importance of constraining radiative feedbacks for accurate projections of circulation changes.

1. Introduction

a. Motivation and aims

Among the most notable aspects of the atmospheric circulation response to CO_2 forcing is the tendency for the midlatitude jets and storm tracks to shift poleward (Kushner et al. 2001; Yin 2005; Barnes and Polvani 2013; Harvey et al. 2014). Future shifts in circulation could have critical implications for weather and climate at regional scales (e.g., Shepherd 2014; Simpson et al. 2015). Unfortunately, however, our understanding of the atmospheric circulation response to CO_2 forcing remains qualitative rather than quantitative, as differences in jet and storm track responses among current climate models are considerable (Barnes and Polvani 2013; Harvey et al. 2014; Ceppi et al. 2014), limiting our ability to anticipate future impacts (Zappa and Shepherd 2017).

To address this issue, it is helpful to think of intermodel spread in circulation changes as resulting from the combination of two distinct effects. The first is associated with the fact that the basic state affects the preferred dynamical modes of variability and modes of response to radiative forcing (Ring and Plumb 2008; Sigmond and Scinocca 2010; Kidston et al. 2010; Barnes and Hartmann 2011; Simpson and Polvani 2016). Differences in resolution, numerical schemes, and physics packages among atmospheric models cause substantial differences in basic climate (e.g., Stevens and Bony 2013; Medeiros et al. 2016), and consequently different models subjected to the same radiative forcing will exhibit different circulation responses. But a second important source of spread in circulation response comes from the radiative change itself, in turn associated with model-dependent effects of CO_2 forcing and climate feedbacks. In this paper, we explore this second source of uncertainty and present the first systematic assessment of the dynamical impact of differences in radiative feedback.

Radiative feedbacks involve the responses of surface albedo, clouds, and water vapor to changes in global-mean temperature and their impacts on the climate system's energy budget. The increase in outgoing longwave radiation associated with surface and atmospheric warming is usually also treated as a feedback. Previous analyses of radiative feedbacks in climate models have

Corresponding author: Paulo Ceppi, p.ceppi@reading.ac.uk

quantified the relative contributions of these processes to global-mean warming: decreasing surface albedo and increasing water vapor concentrations both amplify warming and hence are robust positive feedbacks. While cloud feedback is generally also positive, this feedback can range from near zero to strongly positive in current models, constituting the dominant contribution to intermodel spread in equilibrium climate sensitivity (Cess et al. 1990; Colman 2003; Soden et al. 2008; Andrews et al. 2012; Vial et al. 2013; Caldwell et al. 2016).

Although the thermodynamic implications of these feedbacks are well documented, their dynamical effects remain poorly understood. Because extratropical eddies respond sensitively to changes in baroclinicity, the eddy-driven circulation response may depend more strongly on changes in horizontal temperature gradients than on changes in global-mean temperature (e.g., Chen et al. 2010; Harvey et al. 2014; Ceppi and Hartmann 2016; Grise and Polvani 2016). Consequently, the relative contributions of radiative feedbacks to circulation changes—particularly shifts in extratropical circulation—are unlikely to scale with their relative contributions to global-mean warming. Previous work has shown that anomalous radiative heating due to cloud feedback causes the jets to shift poleward in idealized aquaplanet models (Voigt and Shaw 2015, 2016; Ceppi and Hartmann 2016), primarily owing to shortwave radiative changes (Ceppi and Hartmann 2016), although atmospheric longwave cloud-radiative heating may also contribute to this response (Voigt and Shaw 2015, 2016). In particular, Ceppi and Hartmann (2016) showed that clouds account for most of the poleward shift in extratropical circulation under CO_2 quadrupling in an atmospheric model coupled to a mixed-layer aquaplanet ocean, despite contributing only 25% of the total global surface warming. By contrast, water vapor feedback was found to cause an equatorward shift of midlatitude circulation in Voigt and Shaw (2015), although this study used a prescribed-SST lower boundary and hence did not include the impact of changes in the surface energy budget. Considering that the aforementioned studies of the impacts of feedbacks on circulation were based on idealized aquaplanet climate models, however, it remains unknown to what extent radiative feedbacks may affect extratropical dynamics in climate models with realistic circulation, landmass distribution, and sea surface temperatures.

In this paper we address the following two main questions:

1) What are the contributions of radiative feedbacks by surface albedo, cloud, and water vapor changes to atmospheric circulation shifts under CO_2 forcing?

2) How much of the intermodel spread in midlatitude jet responses is associated with spread in radiative feedbacks?

To answer these questions, we perform climate model experiments with the radiative locking technique, whereby surface albedo, clouds, and water vapor are prescribed in the radiation code only; this allows us to impose the feedbacks as radiative forcings and to decompose the full climate system response to CO_2 forcing into individual contributions of each feedback process (Schneider et al. 1999; Hall and Manabe 1999; Graversen and Wang 2009; Mauritsen et al. 2013). Furthermore, to quantify the impact of model uncertainty in radiative feedback on circulation we carry out "ghost forcing" experiments (Hansen et al. 1997; Alexeev et al. 2005) in which we impose the effect of different radiative feedbacks as prescribed radiative heating anomalies. As we will show, shortwave radiative feedbacks associated with clouds and surface albedo statistically explain about 50% of the spread in jet shift among CMIP5 models based on our experiments; this provides causal support for a previously identified correlation between shortwave changes and Southern Hemispheric jet response in CMIP5 models (Ceppi et al. 2014) and demonstrates the critical importance of radiative feedbacks for intermodel spread in circulation changes.

b. Causal relationships

Before discussing our analysis methods and results, we should consider two difficulties in inferring causal relationships between radiative feedbacks and circulation changes. First, radiative feedbacks can be both a cause and a consequence of circulation changes. The relationship between clouds and the storm track is a helpful example: a poleward shift of the storm tracks could cause cloud-radiative anomalies (Bender et al. 2012; Grise et al. 2013; Boucher et al. 2013), but equally, cloud feedbacks can drive the poleward storm-track shift (Ceppi and Hartmann 2015, 2016). In the context of our study in which feedbacks from different models are prescribed as forcings, causal relationships are clearer because any circulation changes can only be a consequence of the imposed radiative anomalies. However, even in this particular case a correlation between different radiative feedbacks and circulation changes could have two distinct meanings:

1) Intermodel spread in radiative feedback (for example driven by model-specific physical parameterizations) is driving spread in circulation change.

2) Spread in circulation change and radiative feedback is jointly driven by an external source of spread, such as mean-state biases, or differences in CO_2 forcing.

In this case, the radiative response could amplify the spread in circulation change, but without being the primary cause for the spread.

A second difficulty in causally linking radiative feedbacks to circulation changes is related to the fact that feedbacks cannot be considered as being fully independent from one another. Changes in cloud, water vapor, sea ice, and snow cover are all connected through their interactions with temperature and moisture. Both difficulties can be addressed by evaluating the basic physical mechanisms driving the intermodel spread in radiative feedbacks and the extent to which they reflect a fundamental property of the models (e.g., their parameterization schemes). We will discuss in section 6 to what extent the correlations between radiative feedbacks and circulation responses can be interpreted as resulting from causal linkages.

2. Data and methods

a. Climate models

Our results are mainly based on experiments with two coupled climate models: the Community Earth System Model (CESM), version 1.2.2, run with the atmospheric component CAM4 at a resolution of $1.9° \times 2.5°$ (latitude by longitude) with 26 vertical levels (Neale et al. 2010), and the Max Planck Institute (MPI) for Meteorology atmospheric model, version 6.0 (ECHAM6), run at T63 spectral horizontal resolution with 47 vertical levels (Stevens et al. 2013). These atmospheric models were part of the CCSM4 and MPI-ESM-LR fully coupled models used in phase 5 of the Coupled Model Intercomparison Project (CMIP5; Taylor et al. 2012), although for CMIP5 CAM4 was run at a higher horizontal resolution of $0.9° \times 1.25°$. Both atmospheric components are coupled to a slab ocean model with prescribed, monthly varying ocean heat fluxes that do not change between simulations. For CAM4, these heat fluxes were inferred from a preindustrial control simulation coupled to a full dynamical ocean; for ECHAM6, ocean heat transport was derived from a 30-yr simulation with prescribed sea surface temperatures (SSTs) following the Atmospheric Model Intercomparison Project (AMIP) protocol. Both climate models include a representation of sea ice; CAM4 is coupled to a full sea ice model, while ECHAM6's slab ocean model only produces thermodynamic sea ice.

b. Radiative locking method

The impact of radiative feedbacks on atmospheric circulation changes is quantified through the use of radiative locking model experiments (Wetherald and Manabe 1988; Hall and Manabe 1999; Schneider et al.

TABLE 1. List of CAM4 and ECHAM6 simulations. The simulations $1xCO_2$ and $2xCO_2$ are the two reference integrations from which values of surface albedo A, radiative properties of clouds C, and water vapor mixing ratios W are output at every radiative time step. The following 16 simulations have A, C, and W locked to either the $1 \times CO_2$ values (denoted by 1) or $2 \times CO_2$ values (denoted by 2), as explained in section 2b.

Simulation name	No. of spinup years	No. of years after spinup
$1xCO_2$	10	20
$2xCO_2$	20	20
$1xCO_2$-A1C1W1	10	20
$1xCO_2$-A1C1W2	10	20
$1xCO_2$-A1C2W1	10	20
$1xCO_2$-A1C2W2	10	20
$1xCO_2$-A2C1W1	10	20
$1xCO_2$-A2C1W2	10	20
$1xCO_2$-A2C2W1	10	20
$1xCO_2$-A2C2W2	10	20
$2xCO_2$-A1C1W1	10	20
$2xCO_2$-A1C1W2	10	20
$2xCO_2$-A1C2W1	10	20
$2xCO_2$-A1C2W2	10	20
$2xCO_2$-A2C1W1	10	20
$2xCO_2$-A2C1W2	10	20
$2xCO_2$-A2C2W1	10	20
$2xCO_2$-A2C2W2	10	20

1999; Graversen and Wang 2009; Mauritsen et al. 2013; Voigt and Shaw 2015). In locking experiments, values of surface albedo, water vapor concentration, and cloud properties are read in and prescribed in the radiation code only, overriding the values produced by the model. This makes it possible to separately study the radiative impacts of CO_2 forcing, and albedo, cloud, and water vapor feedbacks, as explained below.

The locking technique is implemented in two steps. First, reference experiments are run in which surface albedo values A, radiative properties of clouds C, and water vapor mixing ratios W are saved at every call to the radiation code. Our two reference experiments, termed $1xCO_2$ and $2xCO_2$, are run with CO_2 concentrations of 284.7 and 569.4 ppmv, respectively. In the next step, locked experiments are produced by reading in the time-varying, instantaneous A, C, and W values at every radiative time step from either the $1xCO_2$ or the $2xCO_2$ experiment. For each model, we run all possible combinations of atmospheric CO_2, A, C, and W, yielding a total of 16 experiments. An overview of the simulations is provided in Table 1.

Using our set of experiments, the individual effects of CO_2 forcing and radiative feedbacks can be estimated using pairs of experiments in which only the variable of interest changes, while all other variables are held constant. For example, the difference between experiments $1xCO_2$-A1C2W1 and $1xCO_2$-A1C1W1 (Table 1)
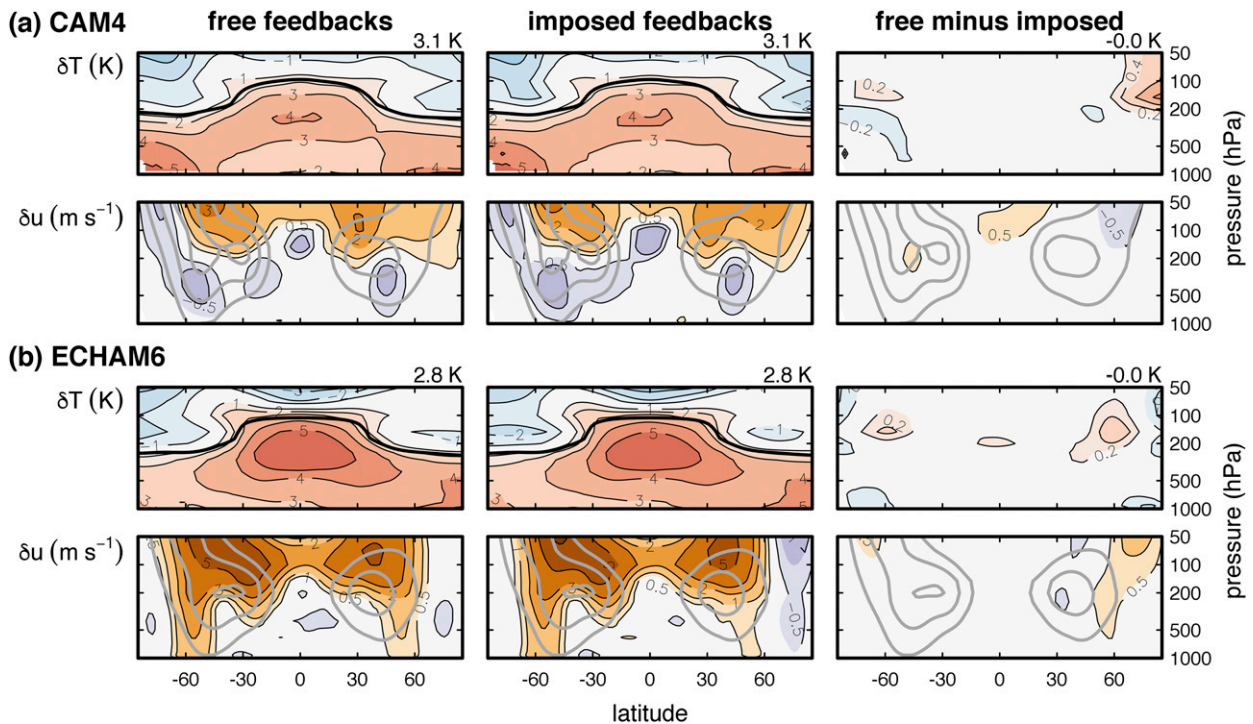
FIG. 1. Zonal-mean temperature and zonal wind response in (a) CAM4 and (b) ECHAM6 CO_2 doubling experiments: (left) the experiments with interactive surface albedo, clouds, and water vapor ("free feedbacks"); (center) the sum of the responses in locking experiments with the feedbacks imposed as forcings ("imposed feedbacks"); (right) the differences between free and imposed feedback responses. Thick gray contours indicate the zonal wind climatology (only positive values shown; contour interval $10 \, \mathrm{m \, s^{-1}}$). The black curves in the temperature plots denote the tropopause height, calculated using the World Meteorological Organization lapse rate definition. Changes in global-mean surface temperature are indicated at the top-right corner of each temperature plot.

provides one estimate of the response to cloud feedback; differencing between 2xCO2-A1C2W1 and 2xCO2-A1C1W1 provides another estimate, but in a warmer state. In total, eight pairs of experiments are available to estimate the response to CO_2 doubling and each of the feedbacks. The results in the paper show the responses averaged over the eight respective pairs of experiments. The full set of differences used to calculate the responses to changes in CO_2, A, C, and W is listed in appendix A (Fig. A1).

When imposing the changes in A, C, and W by the locking method, the resulting radiative changes are no longer feedbacks in the strict sense of the word; the feedbacks are being imposed as forcings. For simplicity, we refer to these radiative responses as "imposed feedbacks." A key assumption is that the sum of the responses to imposed changes in CO_2, A, C, and W is approximately equal to the response to CO_2 forcing with all feedbacks enabled; in other words, we assume that the full climate response to CO_2 doubling can be meaningfully decomposed into partial contributions from individual feedback processes. As shown in Fig. 1, this is indeed the case for both models: the sum of the

responses to individual feedbacks (plus CO_2 doubling with no feedbacks enabled other than temperature feedbacks) compares very favorably with the full response to CO_2 doubling with all feedbacks enabled. Minor differences in the temperature response can be seen at high latitudes, particularly near and above the tropopause; these differences in temperature response are associated with small differences in zonal wind change, which are generally smaller than $0.5 \, \mathrm{m \, s^{-1}}$ except on the poleward flank of the Northern Hemispheric tropospheric jet in ECHAM6. Similar agreement between free and imposed feedback responses is found for other variables such as surface pressure and meridional mass streamfunction (not shown). We therefore conclude that the imposed feedback experiments can be used to partition the dynamical changes associated with CO_2 forcing among individual feedback processes.

c. Ghost forcing experiments

To understand the impact of radiative feedbacks on circulation across a wider range of models, we run CAM4 with prescribed "ghost" forcings (Hansen et al. 1997; Alexeev et al. 2005) that mimic the shortwave

radiative heating anomalies associated with cloud and albedo feedbacks in different CMIP5 models. These ghost forcings are applied as imposed anomalies in radiative heating tendency as a function of longitude, latitude, and month of the year, where the anomalies correspond to the radiative feedback calculated for a given model. The forcings are imposed at the surface, under the assumption that the radiative anomalies diagnosed at the top of atmosphere in CMIP5 models are entirely due to surface radiative changes, which is true to a good approximation for the shortwave anomalies used here (cf. the blue curves in appendix B in Figs. B1a,b; Allan 2011; Previdi and Liepert 2012). Because we are interested in the *absolute* circulation changes rather than changes per degree warming, we use the absolute radiative changes associated with feedback processes (in $W\,m^{-2}$) rather than the radiative feedbacks themselves (in $W\,m^{-2}$ per degree warming) to force CAM4.

Since we wish to quantify the dynamical response to specific feedback processes, we must ensure that CAM4 does not produce any internal radiative feedbacks (other than temperature feedbacks) in response to our ghost forcings, which would introduce additional radiative changes. Therefore, the albedo, cloud, and water vapor fields are locked to their $1 \times CO_2$ climatology in all simulations, suppressing the corresponding feedbacks. This ensures that the responses seen in our experiments are entirely ascribable to the imposed external forcings, rather than to internal feedbacks. Each of the ghost forcing experiments is spun up for 5 years, starting from the equilibrated $1 \times CO_2$ climate, and climatologies are calculated over the following 10 years of integration. We have verified that ghost forcing simulations yield similar results compared with the radiative locking method when imposing CAM4's and ECHAM6's cloud-radiative heating anomalies, and the method successfully replicates the differences in circulation response observed between CAM4 and ECHAM6 (not shown).

d. Atmospheric circulation metrics

In this paper we focus on shifts in zonal-mean circulation, which we quantify with metrics of jet position and edge of the tropics. Prior to calculating the metrics, zonal wind and meridional mass streamfunction values are interpolated onto a 0.1° latitude grid using cubic interpolation. The eddy-driven jet position is defined as the latitude of peak zonal-mean zonal wind at 850 hPa, and the jet speed is simply the zonal wind speed at the jet latitude. The width of the tropics is measured as the latitude where precipitation minus evaporation crosses zero at the poleward edge of the subtropical dry zone and also as the Hadley cell edge latitude (i.e., the

latitude where the mass streamfunction equals zero at 500 hPa). Throughout the paper, circulation shifts are defined as positive poleward.

3. Dynamical response to radiative feedbacks

The contributions of radiative feedbacks to changes in zonal-mean circulation following CO_2 doubling are presented in Fig. 2 for the locking experiments with CAM4 and ECHAM6, and the difference between the two models. In this discussion we mainly focus on the response of the tropospheric eddy-driven jet, since it reflects the overall tendency of the extratropical circulation to shift meridionally. In CAM4, CO_2, albedo, clouds, and water vapor cause very distinct spatial patterns of warming, resulting in widely diverse zonal wind changes. Clouds cause the most pronounced poleward shift in both hemispheres; CO_2 causes little change in zonal wind below the upper troposphere; water vapor produces a strengthening and upward shift of the subtropical jets, along with a weak equatorward shift of the eddy-driven jet in the Southern Hemisphere (SH); and surface albedo forcing yields a marked weakening and equatorward shift of the Southern jet, with a similar but much more muted response in the Northern Hemisphere (NH). The net effect of these various contributions (Fig. 1, center) is mainly a weakening of the tropospheric westerlies in both hemispheres.[1]

Now turning to the ECHAM6 responses (Fig. 2, center), we find substantial differences relative to CAM4 in the temperature and zonal wind responses associated with all three feedbacks, while the effect of CO_2 forcing alone appears more similar. The positive albedo feedback is weaker in ECHAM6 than in CAM4, resulting in less polar warming and no discernible zonal wind response. While clouds still cause a poleward jet shift in both hemispheres, cloud feedback in ECHAM6 causes more pronounced tropical warming and stronger high-latitude cooling in the SH, resulting in more overall strengthening of the midlatitude zonal wind, particularly in the SH. Furthermore, water vapor feedback causes more warming in the tropical free troposphere, resulting in larger strengthening of the upper-tropospheric subtropical winds by thermal wind balance. The net result of these effects is a strengthening and poleward shift of the midlatitude westerlies under CO_2 doubling, especially in

---

[1] This is in contrast to the pure poleward shift produced by the fully coupled version of this model in the abrupt4xCO2 experiment of CMIP5 (not shown). Since the atmospheric component is the same, it is likely that ocean heat transport is responsible for the difference in temperature and circulation responses.
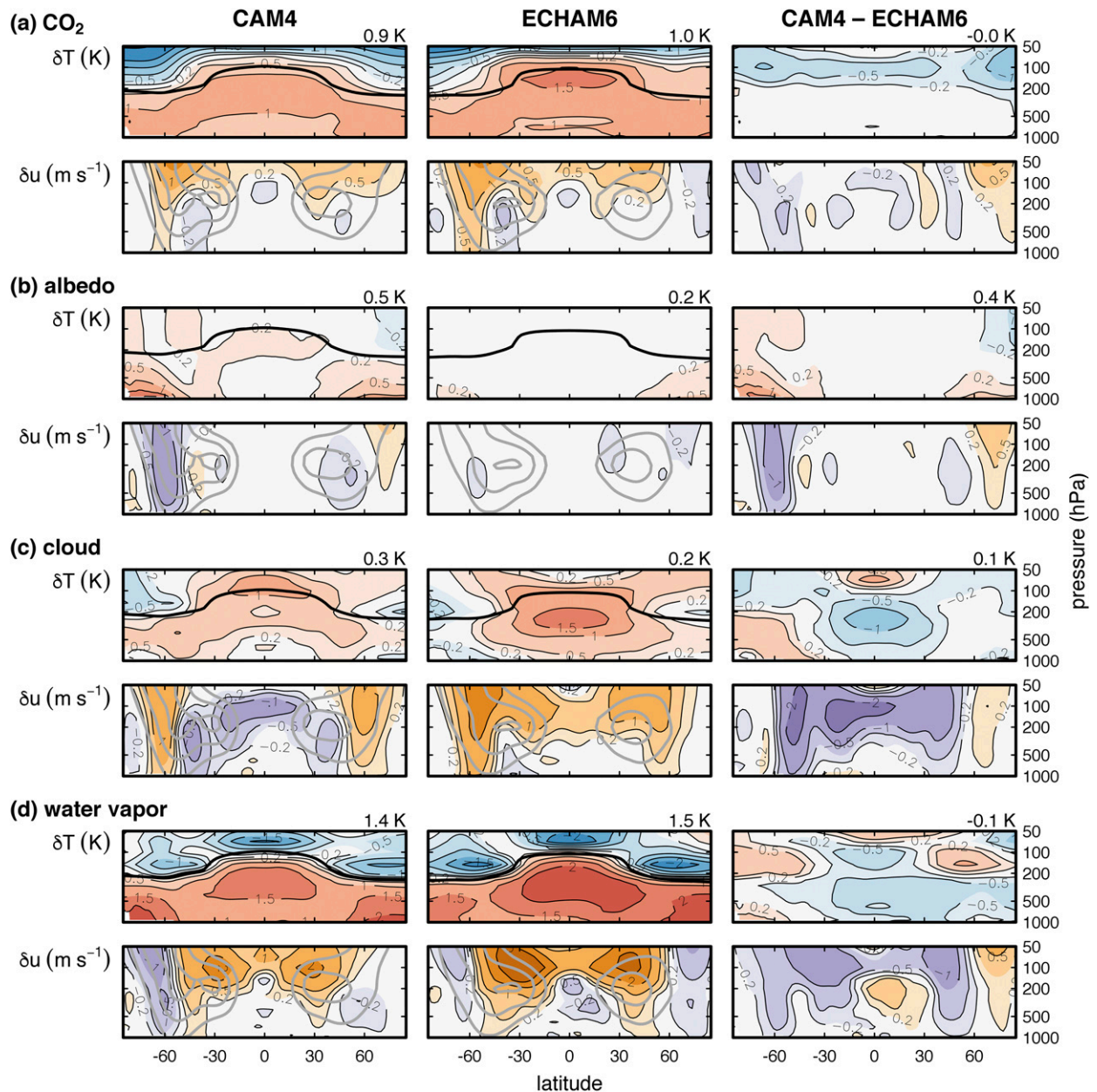
FIG. 2. Zonal-mean temperature and zonal wind responses to (a) CO_2 doubling with no feedbacks and (b)–(d) imposed albedo, cloud, and water vapor feedbacks, respectively. The total response (sum of CO_2 forcing and imposed feedbacks) is shown in Fig. 1, center. Thick gray contours indicate the zonal wind climatology (only positive values shown; contour interval $10 \, \text{m s}^{-1}$). The black curves in the temperature plots denote the tropopause height. Changes in global-mean surface temperature are indicated at the top-right corner of each temperature plot.

the SH, in striking contrast to CAM4's net response (Fig. 1a, center).

The differences in temperature and zonal wind responses between CAM4 and ECHAM6 must be related to differences in magnitude and spatial structure of the radiative feedbacks (discussed in the next subsection), known to be highly model dependent. Differences in the

basic state may also contribute to the discrepancies in dynamical response between the two models, however; CAM4's jets are situated at higher latitude than ECHAM6's (52.9° vs 47.5° in the SH; 48.8° vs 45.2° in the NH) and lower-latitude jets are generally expected to shift poleward more readily as the atmosphere warms (Barnes and Hartmann 2011).
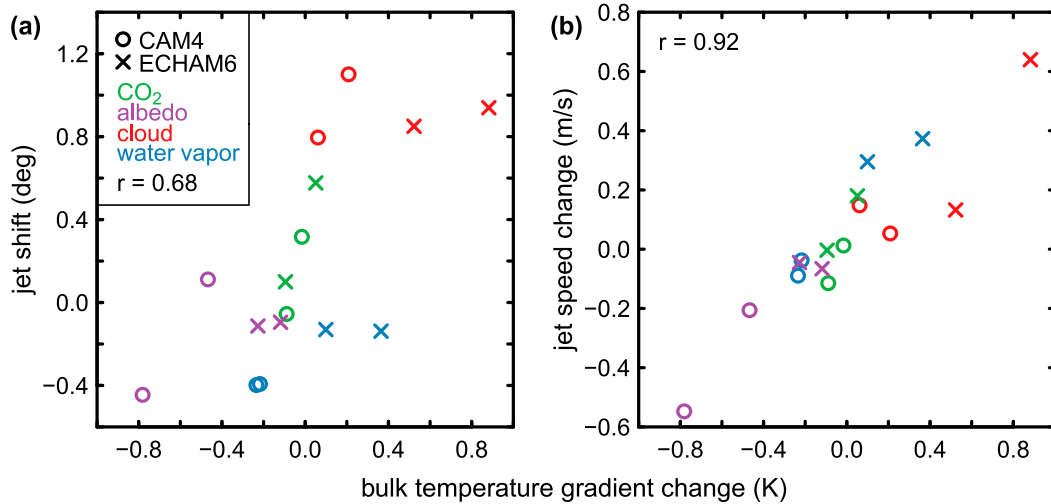
FIG. 3. Relationship between change in bulk tropospheric-mean meridional temperature gradient change and jet response in the imposed feedback experiments. The tropospheric-mean temperature is defined as the mass-weighted vertical average below 200 hPa. The meridional gradient is calculated as the difference in area-averaged temperature between the latitude bands 10°–30° and 60°–90°. The plots include the responses in both hemispheres.

Despite the complexity and diversity of the temperature and zonal wind responses to radiative feedbacks, changes in meridional temperature gradients (i.e., baroclinicity) constitute a reasonably robust mechanism to interpret the differences in midlatitude jet response between experiments and between models, as shown in previous work with idealized and comprehensive models (e.g., Brayshaw et al. 2008; Butler et al. 2010; Chen et al. 2010; Ceppi et al. 2012; Harvey et al. 2014; Zappa and Shepherd 2017). By contrast, the global-mean temperature response is a poor predictor of differences in jet response between CAM4 and ECHAM6, or between imposed feedback experiments (Fig. 2). To highlight the role of baroclinicity changes, we define a bulk meridional temperature gradient as the difference in tropospheric-mean temperature between the tropics (10°–30°) and high latitudes (60°–90°). We use the tropospheric mean (calculated as the mass-weighted vertical average below 200 hPa) since both upper- and lower-level baroclinicity changes have been found to affect the jet in previous work, and we focus on the tropics and high latitudes because these are often regarded as a driver of midlatitude changes (Harvey et al. 2014; Ceppi and Hartmann 2016; Zappa and Shepherd 2017). This simple metric of tropospheric baroclinicity change is a good qualitative predictor of changes in jet latitude and speed (Fig. 3), with increasing baroclinicity favoring a poleward shift and strengthening of the jet. (Note that the results are not sensitive to the exact choice of latitude bands and are robust to the exclusion of outliers.) The relationship is substantially weaker and

less robust for the jet shift than for the change in jet speed, however, explaining less than half of the variance in jet shift ($r^2 = 0.46$); this implies that factors other than the tropospheric-mean meridional temperature gradient must also contribute to the spread in jet shifts seen in Fig. 2. If we separately consider temperature gradient changes in the upper ($500 \geq p \geq 200$ hPa) and lower ($p > 500$ hPa) troposphere, we find a much stronger relationship in the lower troposphere than at upper levels ($r = 0.83$ and 0.28, respectively; not shown). Changes in tropospheric stability (also a component of baroclinicity) may be a further contribution to the circulation shifts shown in Figs. 2 and 3 (e.g., Frierson et al. 2007).

The shifts in zonal-mean circulation caused by CO_2 and the various imposed feedbacks are summarized in Fig. 4. We find coherent responses across metrics of circulation width, showing that the midlatitude jet response is a good indicator for the overall tendency of the circulation to shift meridionally. The metrics of tropical width and jet latitude highlight the dominant contribution of clouds, which alone account for most or all of the poleward expansion of the circulation. [Note that although the net jet response in CAM4 is mainly a weakening (Fig. 1a), the jet shifts poleward because the weakening occurs preferentially on its equatorward flank, especially in the NH.] CO_2 forcing also contributes to the poleward expansion of the Southern Hemispheric circulation in the absence of feedbacks, while surface albedo changes induce an equatorward contraction in CAM4 in the SH. The shifts associated with
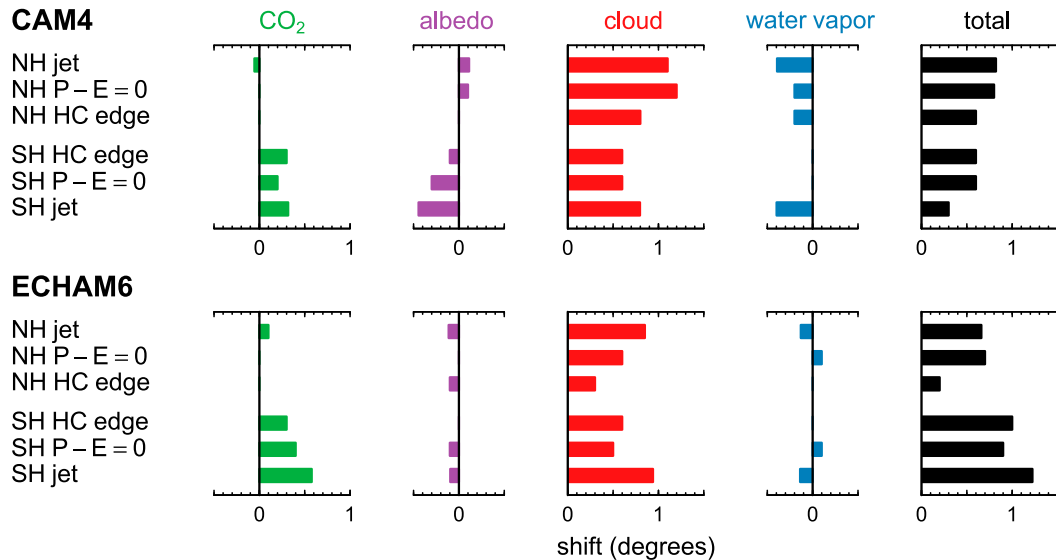
FIG. 4. Shifts in zonal-mean circulation (° lat), quantified by metrics of jet position, edge of the subtropical dry zone, and Hadley cell edge. See section 2d for metric definitions. Positive values denote poleward shifts.

water vapor are negligible in ECHAM6, while weak (<0.5°) equatorward shifts occur in CAM4. The net response is dominated by the poleward-shifting tendency caused by clouds and, to a lesser extent, CO_2, although the mitigating effects of albedo and water vapor in CAM4 are responsible for much of the intermodel differences. While all metrics indicate a poleward shift in the net response, this shift is generally modest (around 1° or less) for a doubling of CO_2 in our two models. However, the total jet shifts are comparable in magnitude to the shifts found in fully coupled abrupt4xCO2 runs (the multimodel mean values being 1.1° in the SH and 0.4° in the NH, after scaling by 0.5 to ensure comparability with our 2xCO2 experiments).

Since the circulation responses shown in Figs. 2–4 are averaged over eight sets of differences between pairs of 20-yr simulations (cf. section 2b), they are robust. The circulation responses to each imposed feedback are generally in reasonable agreement among the eight sets of differences, as discussed in appendix A. This suggests that for this range of radiative perturbations, the circulation is not overly sensitive to the order in which the feedbacks are imposed and to the associated changes in basic state.

4. Feedback analysis

The distinct circulation impacts of albedo, cloud, and water vapor changes reflect differences in the magnitude and spatial pattern of their radiative feedback. To understand how differences in radiative feedback may affect the temperature and circulation responses in our model experiments, in Fig. 5 we compare the meridional feedback patterns produced by CAM4 and ECHAM6 (green and orange curves), diagnosed by offline radiative calculations following the partial radiative perturbation method (Colman and McAvaney 1997). To provide context for our results, we also show feedback values from 28 CMIP5 coupled climate models forced with abrupt CO_2 quadrupling (gray and black curves; models listed in Table 2). The CMIP5 feedbacks are diagnosed with radiative kernels (Soden et al. 2008), and we do not separate feedbacks from rapid adjustments (Andrews and Forster 2008; Gregory and Webb 2008). The response to CO_2 quadrupling is calculated as the change between the piControl climatology of years 1–50 and the abrupt4xCO2 climatology of years 121–140.

While the surface albedo feedback is robustly positive at high latitudes, as expected (Fig. 5a), this feedback is considerably stronger in CAM4 over the high southern latitudes than in ECHAM6. This is consistent with the difference in temperature and circulation responses there (cf. Fig. 2b). Compared with CMIP5, the feedback values over the Arctic in both CAM4 and ECHAM6 are about 3 times smaller; this is likely because the sea ice response scales nonlinearly with CO_2 forcing and global-mean temperature (recall that our experiments are forced with CO_2 doubling, while the CMIP5 experiments use CO_2 quadrupling). This suggests that the climate impacts of Northern Hemispheric surface albedo changes may be substantially larger under CO_2 quadrupling than in the case of doubling.
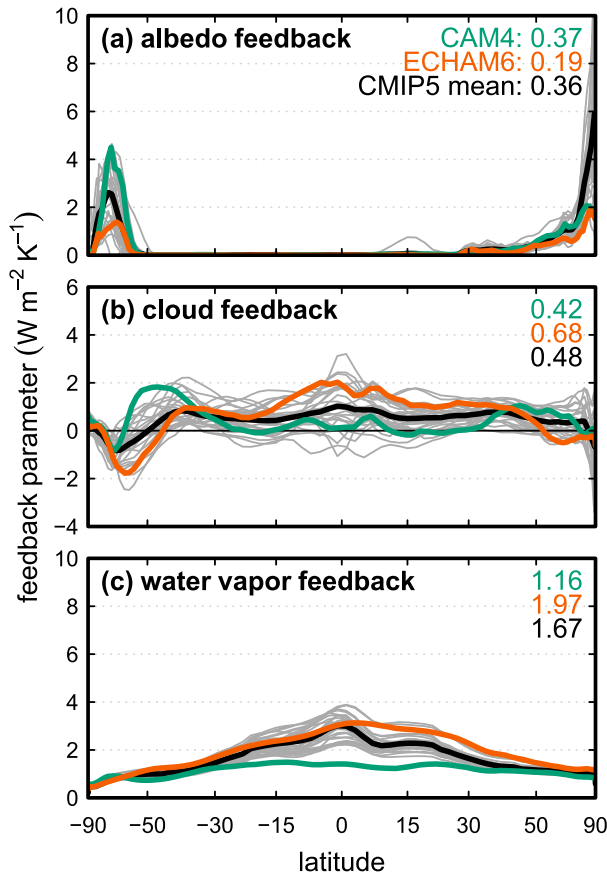
FIG. 5. Zonal-mean radiative feedback at the top of atmosphere in the CAM4 (green) and ECHAM6 (orange) CO_2 doubling experiments, diagnosed from partial radiative perturbation (PRP) experiments. Global-mean values ($W\,m^{-2}\,K^{-1}$) are shown in the top-right corner of each panel. The gray curves denote radiative kernel–based feedback estimates from CMIP5 abrupt4xCO2 experiments (see Table 2 for a list of models), with the multimodel mean shown as a thick black curve. The horizontal axis scales with the sine of latitude to reflect area weighting.

CAM4 and ECHAM6 differ considerably in terms of the cloud feedback (Fig. 5b). In CAM4, the feedback is near zero generally, except for a large positive anomaly between 30° and 60° latitude (especially in the SH) and a weak negative anomaly just poleward of 60°S. By contrast, ECHAM6 produces a positive cloud feedback throughout the tropics and subtropics, while a negative feedback occurs poleward of about 50° latitude. Again, the different meridional patterns of feedback are clearly reflected in the associated temperature responses (Fig. 2c); however, they cannot explain differences in the vertical structure of warming, which are related to the vertical distribution of longwave cloud feedback (Fig. B1). CAM4 and ECHAM6 fall well within the range of cloud feedback values in CMIP5, although the spread is large; generally speaking, cloud feedback in

ECHAM6 presents a larger tropics-to-extratropics gradient than most CMIP5 models, while the converse is true of CAM4.

The water vapor feedback (Fig. 5c) presents a much more consistent meridional structure between models, peaking near the equator and decreasing with latitude. The ECHAM6 water vapor feedback is in broad agreement with the CMIP5 ensemble, but stronger than average in the tropics. By contrast, CAM4 produces a very weak water vapor feedback in the tropics and is an outlier. (We have verified this result using radiative kernels, obtaining very similar values.) The difference in water vapor feedback is reflected in the larger free-tropospheric temperature response to water vapor changes seen in ECHAM6 relative to CAM4 (cf. Fig. 2d). While the differences in cloud and water vapor feedbacks result in large differences in free-tropospheric warming, they cause a similar amount of surface warming (Figs. 2c,d); this is because the feedbacks differ primarily in the atmosphere, while the surface radiative changes are more similar, at least in a global-mean sense (not shown).

The temperature response to water vapor forcing (cf. Figs. 5c and 2d) is characterized by amplified warming in the tropical upper troposphere and in polar regions at lower levels, both of which are fundamental effects of latent heating (resulting from moist convection and poleward latent heat transport, respectively). Owing to this, the lower-level temperature response to water vapor feedback peaks at the poles even though the radiative anomaly peaks in the tropics; the same result applies to CO_2 forcing (not shown). Generally speaking, we expect positive tropical radiative forcings to favor both polar and tropical upper-level amplification, since moister tropical air masses will release more latent energy as they are transported upward or poleward. The enhanced latent energy flux convergence can be offset by local negative feedbacks, however (Roe et al. 2015); as an example, the lack of polar amplification in response to cloud feedback (Fig. 2) is consistent with the local negative feedback, particularly in the SH.

5. Contributions of shortwave feedbacks to model uncertainty in circulation changes

The results in Figs. 2–5 demonstrate that the circulation impact of any particular feedback process can differ substantially between models because of the large uncertainties in radiative feedback. In this section, we seek to quantitatively assess the impacts of differences in feedback on the spread in circulation responses across the CMIP5 models, separately from other sources of spread such as differences in basic state or model

TABLE 2. List of CMIP5 models used in the analysis (expansions of acronyms are available online at http://www.ametsoc.org/PubsAcronymList.). The models are listed along with their global-mean SW radiative changes in the abrupt4xCO2 experiment induced by surface albedo feedback (SW_{alb}) and cloud feedback (SW_{cld}), as well as their SW heating index values for albedo and clouds in each hemisphere. The SW heating index is defined as the difference between area averages over the latitude bands 20°–50° and 50°–90°. The feedbacks are calculated using radiative kernels after Soden et al. (2008). Note that the values shown are absolute radiative changes (W m^{-2}), not normalized by global-mean surface warming. The eight models shown in boldface produce the minimum or maximum value for at least one of the metrics (boldface values). (Expansions of acronyms are available online at http://www.ametsoc.org/PubsAcronymList.)

Model name	SW_{alb}	SW_{cld}	SW_{alb} heating index		SW_{cld} heating index	
			NH	SH	NH	SH
ACCESS1.0	1.77	0.78	−7.77	−4.89	3.73	6.86
ACCESS1.3	1.46	2.65	−6.92	−5.18	3.53	6.23
BCC_CSM1.1	1.57	0.06	−4.84	−6.16	5.52	7.16
BCC_CSM1.1(m)	1.56	1.58	−4.32	−6.20	5.86	7.77
BNU-ESM	**3.30**	0.14	−9.22	**−11.51**	**−0.91**	6.74
CanESM2	1.74	0.36	−5.91	−6.23	0.89	8.00
CCSM4	1.78	0.40	−5.10	−7.91	1.21	4.71
CNRM-CM5	1.95	0.81	−6.24	−6.54	3.07	6.07
CSIRO Mk3.6.0	1.71	2.87	−3.80	−9.13	4.20	10.08
FGOALS-g2	1.94	−0.56	−6.28	−6.96	3.77	3.74
FGOALS-s2	2.11	**−2.67**	−6.17	−8.89	2.61	8.29
GFDL CM3	2.01	3.81	−9.47	−2.32	4.04	8.51
GFDL-ESM2G	0.72	−1.37	−3.23	**−0.39**	6.07	7.75
GFDL-ESM2M	0.85	−1.27	−3.28	−1.37	7.18	7.35
GISS-E2-H	0.99	−2.04	−3.76	−1.89	0.83	**0.14**
GISS-E2-R	**0.63**	−1.80	**−1.88**	−1.36	1.82	0.87
HadGEM2-ES	2.21	1.52	−10.54	−6.49	2.61	7.18
INM-CM4	0.92	−0.88	−1.98	−3.42	1.07	3.35
IPSL-CM5A-LR	1.16	**6.44**	−4.38	−2.68	5.88	**16.18**
IPSL-CM5A-MR	1.05	6.26	−4.51	−1.82	6.62	15.89
IPSL-CM5B-LR	0.95	2.84	−4.02	−1.80	4.62	7.63
MIROC5	1.67	0.55	−8.45	−2.40	0.84	5.73
MIROC-ESM	3.05	2.64	**−10.64**	−10.35	5.30	14.78
MPI-ESM-LR	1.65	1.87	−8.84	−4.08	8.23	10.67
MPI-ESM-MR	1.74	1.61	−8.26	−5.26	6.39	11.00
MPI-ESM-P	1.51	1.62	−6.21	−4.44	**8.46**	10.61
MRI-CGCM3	1.68	1.39	−5.13	−6.39	3.27	3.91
NorESM1-M	1.29	1.10	−5.96	−2.75	0.85	3.81
CMIP5 mean	1.61	1.10	−5.97	−4.96	3.84	7.54

numerics. To this end, we impose radiative feedbacks from a set of CMIP5 models as ghost forcings in CAM4 (section 2c; Hansen et al. 1997; Alexeev et al. 2005).

For practical reasons, in our ghost forcing experiments we use only shortwave (SW) cloud and albedo feedbacks. Unlike longwave (LW) feedbacks and SW water vapor feedback, which have a substantial atmospheric component, SW cloud and albedo feedbacks affect mainly the surface with little impact on the atmospheric energy budget. Using standard CMIP5 output, we are unable to diagnose the vertical structure of atmospheric radiative feedbacks (which are known to contribute to intermodel differences in circulation response to warming in prescribed-SST experiments; Voigt and Shaw 2015, 2016) and hence cannot calculate atmospheric ghost forcing fields. Of the various components of future radiative changes in CMIP5 models,

the SW effects of clouds and albedo are a dominant source of uncertainty in midlatitude baroclinicity changes, as evidenced by the combination of large spread in radiative heating gradient changes and high correlation values with the temperature gradient changes[2] (Table 3). Thus, although we cannot test the impact of all feedbacks on spread in circulation changes, our experiments likely capture a large fraction of the uncertainty in circulation change associated with radiative feedbacks.

Rather than forcing CAM4 with the full set of CMIP5 cloud and albedo SW heating anomalies, we select a

---

[2] Although the same can be said of the Planck feedback (Table 3), this is a response to the spread in warming rather than a driving factor.

TABLE 3. Coefficients of correlation between change in bulk meridional gradient of radiative heating for individual feedbacks and change in tropospheric-mean temperature gradient across all 28 CMIP5 models with abrupt4xCO2 simulations (Table 2). The bulk meridional gradients are calculated by differencing between the 20°–50° and 50°–90° latitude bands, and the tropospheric-mean temperature is the mass-weighted average below 200 hPa (as in Fig. 3).

	Albedo + SW cloud	LW cloud	Water vapor	Lapse rate	Planck
SH std dev ($W\,m^{-2}$)	4.62	1.51	0.69	1.62	3.62
NH std dev ($W\,m^{-2}$)	3.54	1.18	0.64	1.78	3.36
Correlation with SH temp gradient	0.86	−0.47	0.62	0.66	−0.88
Correlation with NH temp gradient	0.70	−0.09	0.80	0.37	−0.73

subset of CMIP5 models representative of the variability across the model ensemble. We select the models based on two metrics: 1) the global-mean SW heating anomaly due to albedo and clouds and 2) the change in bulk meridional gradient of SW heating across the mid-latitudes in each hemisphere [as in Ceppi et al. (2014)]. Here, the bulk meridional gradient is defined as the difference between area averages over the latitude bands 20°–50° and 50°–90°; as will be shown below, these two latitude bands capture the main impacts of SW radiative changes on the jet response. Hereafter the change in bulk meridional SW heating gradient is simply referred to as "SW heating index," and similarly the corresponding change in tropospheric-mean temperature gradient is the "temperature index." We select the models reporting extreme values for either of the metrics (boldface values in Table 2). This yields eight models (BNU-ESM, FGOALS-s2, GFDL-ESM2G, GISS-E2-H, GISS-E2-R, IPSL-CM5A-LR, MIROC-ESM, and MPI-ESM-P)—less than the possible maximum of 12 models because several of the models fulfill

more than one criterion simultaneously. To quantify the average impact of SW changes due to clouds and albedo, we also force CAM4 with the multimodel mean radiative changes (based on all 28 models; Table 2). Since we run separate experiments for albedo and cloud forcing, this yields a total of 18 ghost forcing experiments.

a. Dynamical response to shortwave radiative forcing

To visualize the relationship between the pattern of SW radiative change and zonal wind response, we plot the spatial correlation between anomalous SW heating and jet shift across CAM4 ghost forcing experiments (Fig. 6, left); this includes all 18 experiments with both cloud and albedo forcing. We find that in both hemispheres, increases in subtropical SW heating and decreases in high-latitude heating jointly contribute to poleward jet shifts. Similar (albeit weaker) relationships hold across the whole set of 28 CMIP5 models, particularly in the SH (Fig. 6, center), with a very similar meridional profile of correlation (Fig. 6, right), justifying our choice of latitude bands to calculate meridional
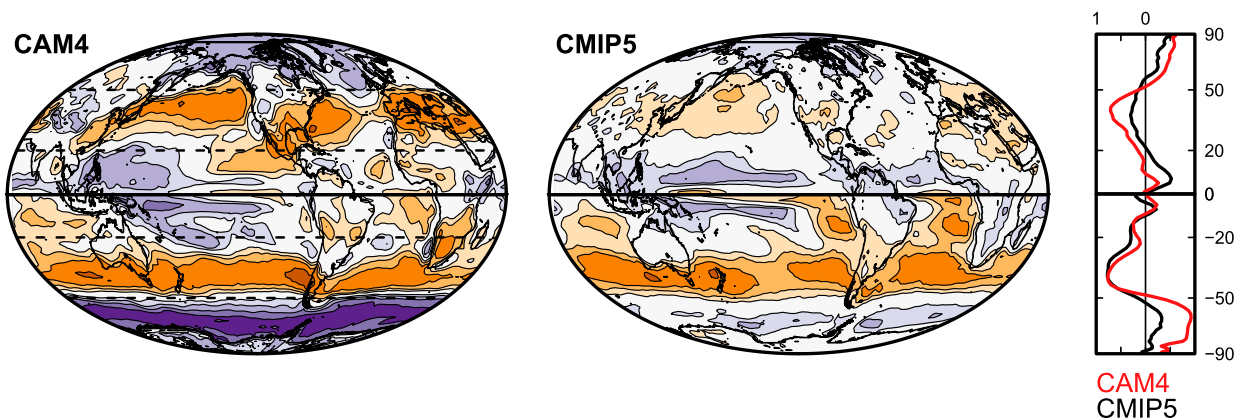

FIG. 6. Correlation coefficient between jet shift (defined as positive poleward) and SW heating anomaly due to albedo and cloud feedbacks at each grid point. Shown are (left) correlations across 18 CAM4 runs with ghost SW forcing (see text), (center) the same calculation for 28 CMIP5 model abrupt4xCO2 runs (Table 2), and (right) the zonally averaged correlations for the CAM4 and CMIP5 runs. The correlation coefficients are separately calculated using NH (top half) and SH (bottom half) jet shift values. In (left), the horizontal dashed lines at 20° and 50° denote the latitude ranges used for the calculation of the surface temperature and net SW radiation indices (see text). The shading interval is 0.2, with absolute values below 0.2 left unshaded.

gradient changes (horizontal dashed lines in Fig. 6, left). This demonstrates that intermodel differences in SW heating due to albedo and cloud feedbacks are sufficiently large to cause detectable differences in jet response to CO_2 forcing in the full CMIP5 ensemble—even in the presence of other important sources of intermodel spread, such as differences in basic state. To illustrate this point, it is worth noting that the eight CMIP5 models used here have a wide range of control SH jet latitudes (from $-42.7°$ to $-49.0°$), spanning 80% of the total CMIP5 spread in the preindustrial control climatology.

In our CAM4 experiments, the correlation pattern is more zonally asymmetric in the NH compared with the SH, likely due to the asymmetries in both radiative feedback and climatological circulation. Such asymmetries also imply that the jet responses may not be entirely expressible as meridional shifts (e.g., Delcambre et al. 2013; Zappa et al. 2015), possibly weakening the relationship between our metric of SW heating gradient anomaly and jet shift. Although we use the zonal-mean zonal wind to define the NH jet for simplicity, qualitatively similar correlation patterns are found if we correlate SW heating anomalies with the North Pacific (140°E–120°W) or North Atlantic (60°W–60°E) jet shift, but with weaker correlations for the North Pacific jet.

The results so far suggest the following mechanism linking the intermodel spread in SW feedbacks to the spread in jet shift: changes in the meridional gradient of SW heating (quantified by the SW heating index) drive changes in midlatitude baroclinicity, which in turn drive changes in the midlatitude zonal winds. The more positive the SW heating index is, the larger the baroclinicity increase is and the stronger the tendency for the jet to shift poleward. We verify these causal linkages by plotting the temperature index, jet shift, change in jet speed, and change in peak eddy kinetic energy (EKE) at 850 hPa against the SW heating index associated with albedo and clouds in our CAM4 ghost forcing experiments (Fig. 7). Here $EKE \equiv \overline{u'^2} + \overline{v'^2} = (\overline{uu} - \overline{u}\,\overline{u}) + (\overline{vv} - \overline{v}\,\overline{v})$, where overbars denote time averages and primes are deviations therefrom.

As expected, we observe a very close positive relationship between SW heating index and temperature index in each hemisphere (Fig. 7a). Cloud and albedo feedbacks have opposing effects on the midlatitude temperature gradient, suggesting a tug-of-war on midlatitude baroclinicity between cloud and albedo SW feedbacks. Consistent with the correlations in Fig. 6, the midlatitude jets also shift in accord with the changes in SW heating and temperature gradients, especially in the SH (Fig. 7b). It is noteworthy that the jet response to SW cloud feedback is generally positive, consistent with the sign of SW heating gradient changes. In particular, the multimodel mean SW cloud feedback causes a poleward jet shift in both hemispheres (black crosses). By contrast, the jet systematically shifts equatorward in response to albedo ghost forcings. Furthermore, SW heating changes also have a clear effect on jet speed (Fig. 7c) and midlatitude storminess, as quantified by the peak value of 850-hPa EKE (Fig. 7d): positive SW heating index and baroclinicity change lead to increasing midlatitude jet speed and EKE, and these effects are stronger in the SH than in the NH. We speculate that the difference is related to the higher degree of zonal symmetry of the SH circulation.

In our ghost forcing experiments, strong correlations between SW heating and circulation changes are expected by construction because the SW anomalies are the only forcing. However, Fig. 6 demonstrates that the meridional gradient of the heating accounts for most of the differences in jet response. Importantly, the jet responses do not correlate well with the changes in global-mean SW heating: for jet shifts we find -0.23 and -0.05 in the SH and NH, respectively, while for jet speed changes the values are -0.16 and -0.35. Furthermore, the correlation coefficient between SW heating index and global-mean surface warming is near zero or negative in our ghost forcing experiments as well as across CMIP5 models (not shown), meaning that the relationships in Figs. 6 and 7 cannot be explained by differences in global-mean warming. Taken together, these results confirm the idea that temperature gradient changes are more critical for the midlatitude circulation response than changes in global-mean temperature (Grise and Polvani 2016). Hence, while constraining the global-mean value of SW feedbacks will reduce uncertainty in climate sensitivity estimates (Cess et al. 1990; Caldwell et al. 2016), it will be equally important to correctly predict the spatial pattern of these feedbacks for improved projections of atmospheric circulation changes.

b. Intermodel spread in jet shift in CMIP5

The results in Fig. 7 have shown that differences in SW albedo and cloud feedbacks can cause a variety of midlatitude jet responses to greenhouse gas forcing. This means that even in the absence of any other sources of intermodel spread (such as differences in basic state or in model numerics), CMIP5 models would still exhibit substantial spread in jet responses just because of the large differences in SW feedback by albedo and clouds. We therefore ask, can our CAM4 ghost forcing results explain part of the CMIP5 spread? If the answer is yes, this would provide additional direct evidence for SW feedbacks driving the intermodel spread in jet response.
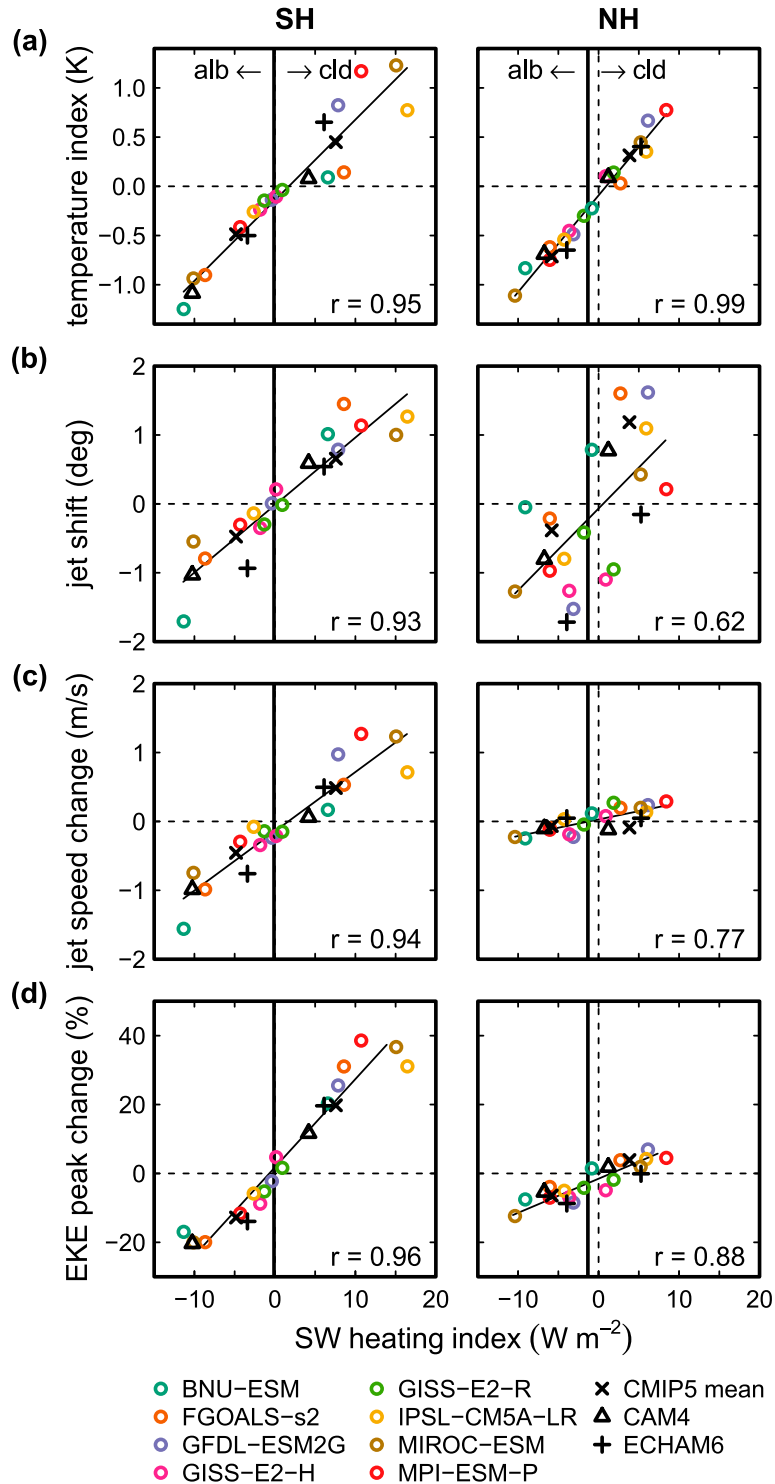
FIG. 7. Scatterplots of (a) temperature index, (b) jet shift (positive poleward), (c) change in jet speed, and (d) change in peak EKE intensity at 850 hPa, against the change in SW heating index for the CAM4 ghost forcing experiments for the (left) SH and (right) NH. The vertical bars separate the responses to albedo forcing (causing a SW heating index decrease) from the responses to cloud forcing (mainly causing a SW heating index increase). The temperature index is based on tropospheric-mean temperature, vertically averaged below 200 hPa. Prior to calculating the indices, the CAM4 and ECHAM6 responses to CO_2 doubling are multiplied by a factor of 2 to make them comparable to the CMIP5 CO_2 quadrupling experiments. Regression lines are calculated by orthogonal (rather than least squares) regression.

We first consider the extent to which the combined effect of SW albedo and cloud feedbacks can account for the spread in baroclinicity changes across CMIP5 abrupt4xCO2 model simulations (Fig. 8a). We find a high correlation in temperature index between CMIP5 and CAM4 simulations, particularly in the SH where virtually all of the spread in temperature gradient change is accounted for by SW heating anomalies associated with cloud and albedo feedbacks. We also note that CAM4 underestimates the intermodel spread in temperature index, as indicated by the regression slopes being larger than one (see discussion below). The strong temperature relationships are consistent with the fact that SW cloud and albedo feedbacks jointly constitute a dominant contribution to intermodel variance in temperature gradient responses (Table 3). Apart from radiative feedbacks, additional spread in atmospheric heating could arise from differences in the meridional structure of CO_2 forcing or changes in ocean heat flux convergence; such effects could explain the weaker correlation in temperature index between CMIP5 and CAM4 in the NH compared with the SH.

Consistent with the relationships found for baroclinicity, the CAM4 ghost forcing experiments statistically explain a large fraction of the variance in CMIP5 abrupt4xCO2 jet shifts and jet speed changes ($r^2 \approx 50\%$, excluding the NH jet speed response; Figs. 8b,c), confirming the causal link between spread in SW feedbacks and spread in jet response.[3] This agrees with earlier results by Ceppi et al. (2014), who compared atmosphere-only simulations with a prescribed SST increase (in which SW feedbacks cannot affect surface temperatures) with greenhouse gas–forced coupled experiments for the same CMIP5 models to demonstrate the role of clouds and albedo in driving the spread in SH jet responses. We note that the CMIP5 jet shifts are systematically positive while the CAM4 responses can have either sign, indicating a robust positive contribution to jet shifts in the CMIP5 abrupt4xCO2 experiments that is not present in our ghost SW forcing experiments, possibly associated with CO_2 (cf. Fig. 4). Furthermore, Fig. 8 also indicates that although the impacts of SW albedo and cloud feedbacks on baroclinicity and the jet tend to cancel each other in the multimodel mean in both hemispheres (cf. Figs. 7a–c), typically they do not cancel out for individual models, because the SW

heating indices for albedo and cloud feedbacks are only weakly correlated (-0.33 and 0.03 in the SH and NH, respectively). Hence, albedo and clouds jointly cause a large spread in jet responses.

The slopes of the temperature relationships in Fig. 8a generally indicate that the meridional temperature gradient is more sensitive to SW forcing in the CMIP5 ensemble than in CAM4. This is likely due to constructive interactions with the high-latitude lapse rate and water vapor feedbacks, which are known to contribute to intermodel spread in polar amplification (Pithan and Mauritsen 2014). In support of this idea, the SW heating index is positively correlated with an index based on the sum of the lapse rate and water vapor feedbacks (0.69 and 0.84 in the SH and NH, respectively) across the eight CMIP5 models included in Fig. 8. Other terms in the atmospheric energy budget, such as LW cloud feedbacks and ocean heat convergence changes, could also interact with the SW forcing and contribute to the difference in sensitivity in Fig. 8a. Despite the larger spread in temperature gradient changes in CMIP5, we do not see a corresponding systematically larger spread in jet responses (Figs. 8b,c), since the slopes can be both much larger or much smaller than one. We therefore deduce that the slopes of the jet responses are dominated by the sensitivity of CAM4's circulation to SW heating by cloud and albedo feedbacks, which depending on the metric of interest may be larger or smaller than the bulk of CMIP5 models.

6. Discussion

a. Coupling between cloud feedback and circulation

In discussing the relationship between radiative feedbacks and circulation, so far we have only considered how albedo, cloud, and water vapor changes affect circulation; we have not discussed how circulation itself can change these fields. Although our experiments demonstrate that intermodel differences in radiative feedbacks lead to a spread in circulation changes, the feedbacks may not be the primary cause of the spread if they are mainly driven by circulation, as discussed in section 1b. While it seems safe to assume that intermodel differences in albedo and water vapor responses are primarily tied to temperature rather than circulation changes, it is not a priori obvious whether the differences in cloud feedback are a cause or a consequence of the different jet responses.

While earlier studies have proposed observational and modeling evidence for poleward jet stream shifts causing cloud feedback around the midlatitudes, as clouds shift to latitudes of weaker insolation (Bender et al. 2012; Grise et al. 2013; Boucher et al. 2013), current evidence suggests that circulation shifts cannot account

---

[3] If we separately consider the responses to cloud and albedo feedbacks in CAM4, we find that both components contribute substantially to the spread of jet responses in CMIP5, except for the SH jet shift where the albedo changes only account for about 5% of the variance in responses (not shown).
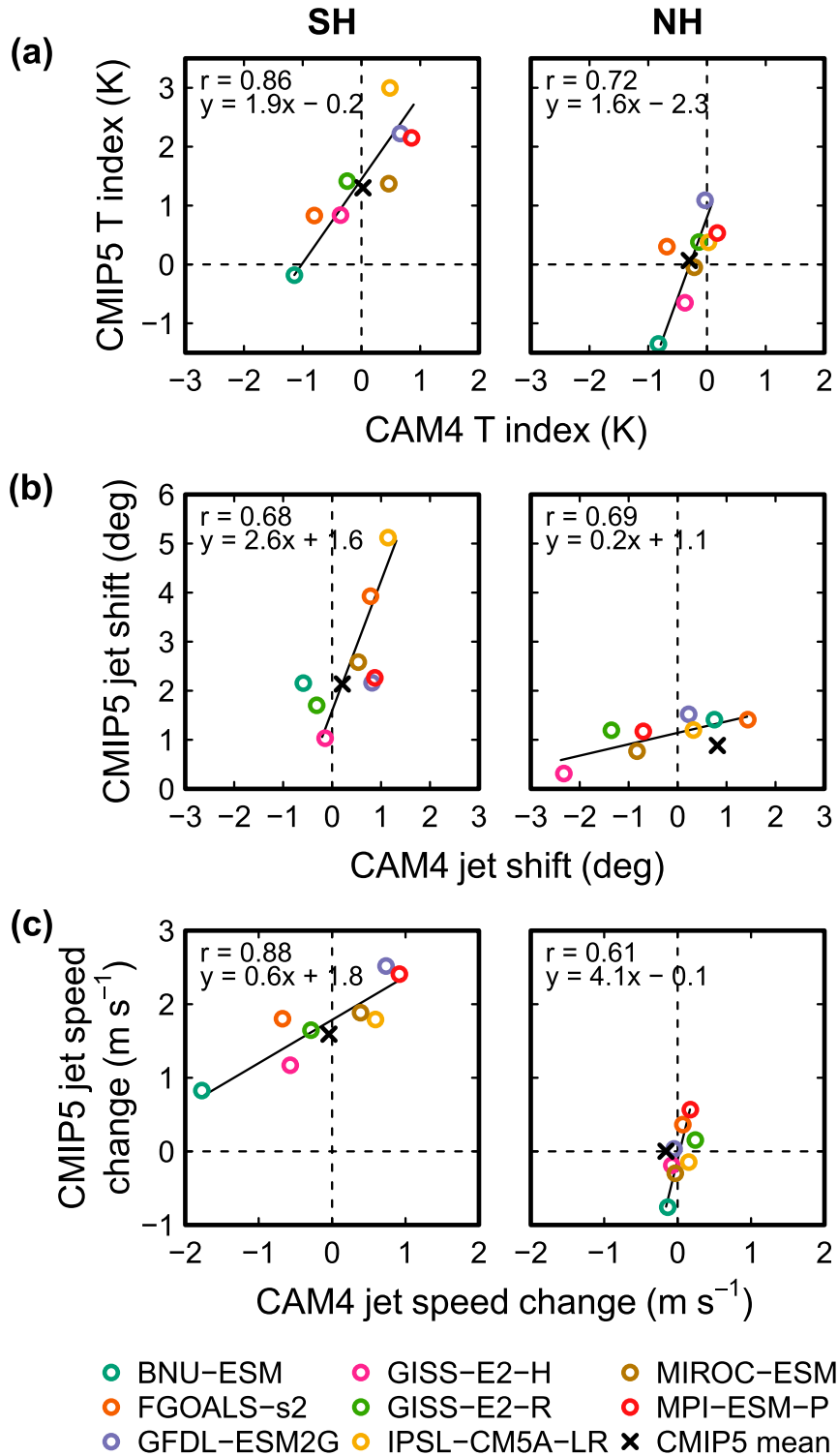
FIG. 8. Scatterplots of (a) temperature index, (b) jet shift, and (c) change in jet speed in CMIP5 abrupt4xCO2 simulations vs CAM4 ghost forcing experiments. The CAM4 results are the sum of the responses due to imposed albedo and cloud feedbacks. The jet shifts are defined as positive poleward. Orthogonal least squares regression lines are plotted, with the equation shown in the top-left corner of each panel.

for cloud feedbacks under global warming (Kay et al. 2014; Ceppi et al. 2014; Ceppi and Hartmann 2015; Grise and Medeiros 2016). Both observations and high-resolution models suggest that subtropical cloud feedbacks will be driven primarily by thermodynamic processes, rather than by dynamical changes (Rieck et al. 2012; Bretherton 2015; Qu et al. 2015; Brient and Schneider 2016), while from middle to high latitudes (poleward of ~45°) increases in the fraction of liquid to total cloud water with warming account for the negative cloud feedbacks (Tsushima et al. 2006; Gordon and Klein 2014; McCoy et al. 2015; Ceppi et al. 2016a). The magnitude of the cloud response strongly depends on how model-specific parameterizations respond to changes in the large-scale environment (Sherwood et al. 2014; McCoy et al. 2015; Brient et al. 2016), as evidenced by single-column model experiments in which the models' cloud schemes are forced with idealized, prescribed boundary conditions (Neggers 2015; Dal Gesso et al. 2015). This suggests that, to first order, cloud feedbacks can be regarded as properties of the models' response to warming, and therefore as primary drivers of intermodel spread.

b. Interactions between radiative feedbacks

Although the locking method allows us to separately impose the radiative effects of changes in albedo, clouds, and water vapor, in reality these responses cannot be regarded as being fully independent. In particular, the water vapor response is strongly dependent on temperature following the Clausius–Clapeyron relationship, and hence depends on heating anomalies associated with CO_2 forcing and with other feedbacks. Cloud feedback is known to interact with ice and albedo changes at high latitudes (Mauritsen et al. 2013), while the upward shift of high clouds, responsible for the positive LW cloud feedback (see appendix B), may depend on the amount of upper-tropospheric warming, for which the water vapor feedback should play an important role (Held and Soden 2000). This idea is supported by the correlations found between lapse rate, water vapor, and LW cloud feedbacks across CMIP5 models (Caldwell et al. 2016). The interdependence of feedbacks means that care is required when inferring causal relationships between feedback processes and circulation changes. Alternative feedback decompositions, for example by counting the change in water vapor under constant relative humidity as part of the temperature response (Ingram 2010; Held and Shell 2012; Ingram 2013), may provide additional physical insight into the processes driving intermodel spread in the response to CO_2 forcing, but may not be straightforward to implement in locking experiments.

Of all the pairwise correlations between albedo, cloud, and water vapor heating indices across the full set of 28 CMIP5 models, only the relationship between cloud and water vapor heating indices is significant ($r = 0.77$ and 0.49 in the SH and NH, respectively), due to the SW component of cloud feedback ($r = 0.73$ and 0.62 between SW cloud and water vapor heating indices). This suggests that water vapor changes amplify the impact of SW cloud feedback on temperature gradients and circulation. Consequently, we expect that the intermodel spread in temperature gradient changes associated with SW cloud feedback would be even larger if the water vapor response under constant relative humidity were treated as part of the temperature response to cloud changes.

c. Role of ocean heat transport

Recent work has demonstrated that the climate system response to localized extratropical radiative forcing, for example due to changes in sea ice (Deser et al. 2015; Tomas et al. 2016) or cloudiness (Kay et al. 2016; Hawcroft et al. 2017), can be dramatically altered by the effect of ocean heat transport changes. Hence, the contributions of feedbacks to changes in temperature and circulation may be different when including the effects of ocean heat transport. Nevertheless, the results shown in Fig. 8 suggest that changes in ocean heat transport are not a dominant driver of changes in midlatitude baroclinicity, since our model experiments with prescribed ocean heat transport can reproduce the CMIP5 spread in temperature gradient changes.

7. Conclusions

We quantify the contributions of radiative feedbacks to midlatitude circulation shifts under CO_2 forcing by imposing the feedbacks as external forcings in two climate models, CAM4 and ECHAM6, both coupled to a slab ocean. This is achieved by directly prescribing ("locking") the albedo, cloud, and water vapor fields in the radiation code. The main findings can be summarized as follows:

- The effect of radiative feedbacks on midlatitude circulation can be interpreted broadly in terms of baroclinicity changes: increasing baroclinicity favors a strengthening and poleward shift of the jet, and vice versa. By contrast, the circulation changes do not scale well with the relative contributions of the feedbacks to global-mean warming.
- In our two models, cloud feedbacks act to enhance midlatitude baroclinicity and cause poleward jet shifts, whereas albedo changes have an opposite (but weaker) impact. Water vapor changes induce opposing changes

in upper- and lower-level baroclinicity, with a weak net impact on the jet.

- Latent heating has a considerable impact on the temperature and circulation responses to radiative heating changes. Anomalous radiative heating in the tropics favors amplified tropical upper-level warming (owing to moist convection) and polar lower-level amplification (owing to poleward latent heat transport). As a result, the spatial structure of the temperature response can differ substantially from that of the radiative anomaly.
- SW cloud and albedo feedbacks cause large uncertainty in baroclinicity changes across CMIP5 models. When forced with SW feedbacks from a set of eight representative CMIP5 models, CAM4 produces a wide range of jet responses that strongly correlate with the meridional gradient of the anomalous shortwave heating. Differences in shortwave feedbacks statistically explain about 50% of the intermodel spread in CMIP5 jet shifts for our set of models. These differences in shortwave feedbacks are uncorrelated with intermodel differences in global-mean warming.

The results in this paper provide the first direct quantification of the impact of climate feedbacks on midlatitude circulation in comprehensive models. Future work should also consider the effect of atmospheric feedbacks, mainly associated with LW heating by water vapor and clouds, on intermodel differences in jet response (Voigt and Shaw 2015, 2016).

An important implication of our results is that observational constraints on radiative feedbacks (e.g., Hall and Qu 2006; Klein and Hall 2015) may help constrain aspects of the dynamical response to greenhouse gas forcing. Such observational constraints, typically derived from short-term (from daily to seasonal) variability, have been proposed for the low-latitude SW cloud feedback by marine low clouds (Qu et al. 2014; Brient and Schneider 2016; McCoy et al. 2017), the high-latitude SW cloud feedback (Gordon and Klein 2014; Ceppi et al. 2016b), and the snow–albedo feedback over land (Hall and Qu 2006; Qu and Hall 2014). Uncertainties remain large, however, and we remain far from being able to constrain the full meridional structure of radiative feedbacks and the associated dynamical impacts. Until more accurate observational constraints are developed, it will therefore remain necessary to take into account the dynamical uncertainties associated with future changes in radiative heating by feedback processes.

APPENDIX A

State Dependence of the Circulation Response

Figure A1 provides a list of the pairs of simulations used to compute the responses to CO_2 forcing and imposed feedbacks (see Table 1 for a list of the locked simulations), with the associated global-mean surface temperature responses and jet shifts. Setting aside any possible impacts of natural variability, differences in temperature and circulation response could occur for two main reasons: first, because the radiative impact of changing CO_2, albedo, cloud, and water vapor fields will slightly vary between experiments; second, because even for a fixed radiative forcing the dynamical response will depend on the basic state. However, Fig. A1 shows that the differences between imposed feedbacks are robust and not strongly dependent on the basic state; hence the results do not rely on the order in which feedbacks are imposed.

The largest variation between simulations is found for the NH jet response in CAM4, where the response often changes sign between pairs of simulations. Even here, however, the effect of clouds clearly stands out as the dominant contribution to a poleward jet shift. For each forcing, the variations in NH jet shift between pairs of CAM4 simulations correlate positively with the bulk temperature gradient change as defined in Fig. 3 (not shown), suggesting that the variability in response is at least in part due to differences in radiative forcing rather than only resulting from dynamical sensitivity to the basic state, although natural variability may also play a role. While we have not investigated the exact causes for the differences in forcing, variations are expected
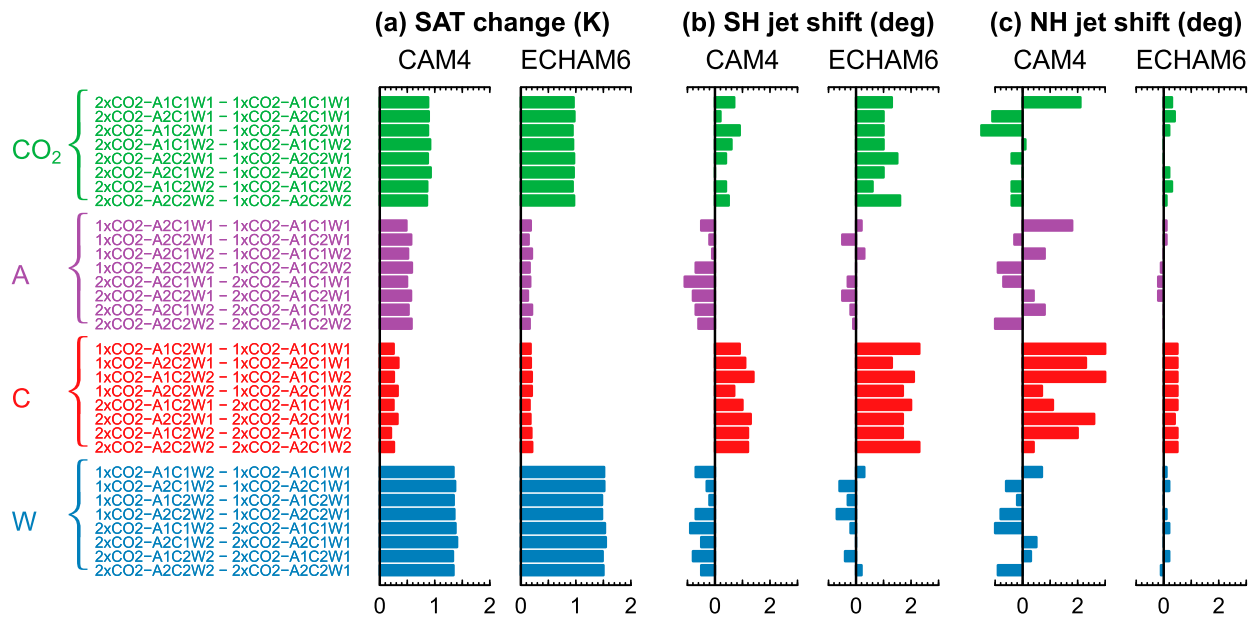
FIG. A1. Change in (a) global-mean surface air temperature, and jet shift in the (b) SH and (c) NH in the full set of locked simulations used to calculate the response to CO_2 forcing and imposed feedbacks; A, C, and W stand for albedo, cloud, and water vapor imposed feedbacks. Jet shifts are positive poleward.

because the radiative impact of changing albedo, clouds, and water vapor depends on the background state. For example, a brightening of high-latitude clouds will have a stronger impact if the clouds overlie a dark ice-free surface (the A2 albedo distribution) than a bright, ice-free one (the A1 distribution); similar interactions occur for other feedbacks.

APPENDIX B

Cloud-Induced Radiative Heating Changes

Figure B1 shows the radiative anomalies associated with cloud feedback in CAM4 and ECHAM6, diagnosed by running the radiation code offline following the partial radiative perturbation methodology (Colman and McAvaney 1997). The top-of-atmosphere (TOA) changes shown in Fig. B1a indicate the effect of clouds on the climate system's energy budget. This effect can be partitioned into radiative changes at the surface (Fig. B1b) and in the atmosphere (Fig. B1c). The atmospheric heating anomalies are essentially due to LW cloud feedback, since clouds cause little SW heating within the atmosphere (consistent with the blue curves being nearly identical in Figs. B1a and B1b). In this appendix we briefly discuss the partitioning of cloud-radiative changes between the surface and the atmosphere and explain the main mechanisms responsible for the radiative changes.

At the TOA, most of the radiative change is associated with the SW effect of clouds (blue and black curves); in particular, SW changes explain the meridional structure of cloud feedback. LW radiative changes tend to oppose the effect of SW radiation, but are weaker at the TOA. At the surface, LW changes oppose SW changes much more strongly, particularly from middle to high latitudes. This is because changes in LW heating by low clouds affect mainly the surface, and the surface and atmospheric effects tend to cancel in the TOA radiative budget. As an example, in CAM4 LW cooling by lower-tropospheric clouds increases strongly poleward of 60° (Fig. B1c) because warming causes an increase in the liquid water content of mixed-phase low clouds, making clouds more emissive (e.g., Tsushima et al. 2006; Kay et al. 2014; Wall and Hartmann 2015; Ceppi et al. 2016a). Much of the enhanced emission of LW radiation goes to the surface, where it causes warming (Fig. B1b).

The increase in high-latitude liquid water content is a robust mechanism that is also responsible for the negative SW cloud feedback found in all current climate models poleward of about 45°–60° (cf. Fig. 5b; Zelinka et al. 2012; Ceppi et al. 2016a). At lower latitudes, most climate models predict a positive SW cloud feedback due to decreases in low cloud fraction, although this effect varies considerably between models and accounts for most of the intermodel spread in net global-mean cloud feedback (Bony et al. 2006; Zelinka et al. 2012;
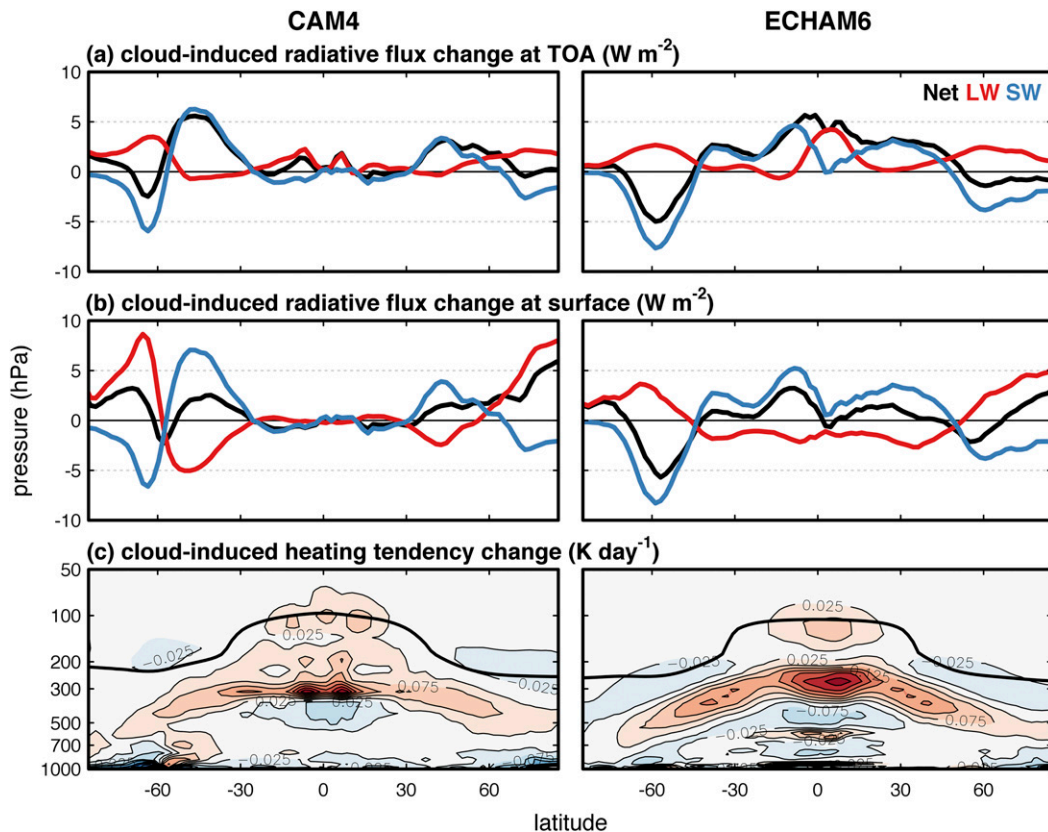
FIG. B1. Change in radiative flux at (a) TOA and (b) surface and (c) atmospheric radiative heating tendency change induced by cloud changes. In (a) and (b), the curves denote LW (red), SW (blue), and net (black) changes. The black curves in (a) are identical to the cloud feedback in Fig. 5, except the changes are not normalized by global-mean surface warming. The black curves in (c) denote the tropopause height. The cloud-induced radiative response was obtained from PRP experiments.

Vial et al. 2013; Caldwell et al. 2016). The atmospheric radiative heating anomalies are dominated by the LW effect of rising high clouds, consistent with the fixed anvil temperature hypothesis (Hartmann and Larson 2002; Zelinka and Hartmann 2010), a robust mechanism favoring a global-mean positive LW cloud feedback in climate models.

REFERENCES

Alexeev, V. A., P. L. Langen, and J. R. Bates, 2005: Polar amplification of surface warming on an aquaplanet in ghost forcing experiments without sea ice feedbacks. *Climate Dyn.*, **24**, 655–666, doi:10.1007/s00382-005-0018-3.

Allan, R. P., 2011: Combining satellite data and models to estimate cloud radiative effect at the surface and in the atmosphere. *Meteor. Appl.*, **18**, 324–333, doi:10.1002/met.285.

Andrews, T., and P. M. Forster, 2008: CO_2 forcing induces semi-direct effects with consequences for climate feedback interpretations. *Geophys. Res. Lett.*, **35**, L04802, doi:10.1029/2007GL032273.

——, J. M. Gregory, M. J. Webb, and K. E. Taylor, 2012: Forcing, feedbacks and climate sensitivity in CMIP5 coupled atmosphere–ocean climate models. *Geophys. Res. Lett.*, **39**, L09712, doi:10.1029/2012GL051607.

Barnes, E. A., and D. L. Hartmann, 2011: Rossby wave scales, propagation, and the variability of eddy-driven jets. *J. Atmos. Sci.*, **68**, 2893–2908, doi:10.1175/JAS-D-11-039.1.

——, and L. Polvani, 2013: Response of the midlatitude jets and of their variability to increased greenhouse gases in the CMIP5 models. *J. Climate*, **26**, 7117–7135, doi:10.1175/JCLI-D-12-00536.1.

Bender, F. A.-M., V. Ramanathan, and G. Tselioudis, 2012: Changes in extratropical storm track cloudiness 1983–2008: Observational support for a poleward shift. *Climate Dyn.*, **38**, 2037–2053, doi:10.1007/s00382-011-1065-6.

Bony, S., and Coauthors, 2006: How well do we understand and evaluate climate change feedback processes? *J. Climate*, **19**, 3445–3482, doi:10.1175/JCLI3819.1.

Boucher, O., and Coauthors, 2013: Clouds and aerosols. *Climate Change 2013: The Physical Science Basis*, T. F. Stocker et al., Eds., Cambridge University Press, 571–657, doi:10.1017/CBO9781107415324.

Brayshaw, D. J., B. Hoskins, and M. Blackburn, 2008: The storm-track response to idealized SST perturbations in an aquaplanet GCM. *J. Atmos. Sci.*, **65**, 2842–2860, doi:10.1175/2008JAS2657.1.

Bretherton, C. S., 2015: Insights into low-latitude cloud feedbacks from high-resolution models. *Philos. Trans. Roy. Soc.*, **373A**, 3354–3360, doi:10.1098/rsta.2014.0415.

Brient, F., and T. Schneider, 2016: Constraints on climate sensitivity from space-based measurements of low-cloud reflection. *J. Climate*, **29**, 5821–5835, doi:10.1175/JCLI-D-15-0897.1.

——, ——, Z. Tan, S. Bony, X. Qu, and A. Hall, 2016: Shallowness of tropical low clouds as a predictor of climate models' response to warming. *Climate Dyn.*, **47**, 433–449, doi:10.1007/s00382-015-2846-0.

Butler, A. H., D. W. J. Thompson, and R. Heikes, 2010: The steady-state atmospheric circulation response to climate change–like thermal forcings in a simple general circulation model. *J. Climate*, **23**, 3474–3496, doi:10.1175/2010JCLI3228.1.

Caldwell, P. M., M. D. Zelinka, K. E. Taylor, and K. Marvel, 2016: Quantifying the sources of intermodel spread in equilibrium climate sensitivity. *J. Climate*, **29**, 513–524, doi:10.1175/JCLI-D-15-0352.1.

Ceppi, P., and D. L. Hartmann, 2015: Connections between clouds, radiation, and midlatitude dynamics: A review. *Curr. Climate Change Rep.*, **1**, 94–102, doi:10.1007/s40641-015-0010-x.

——, and ——, 2016: Clouds and the atmospheric circulation response to warming. *J. Climate*, **29**, 783–799, doi:10.1175/JCLI-D-15-0394.1.

——, Y.-T. Hwang, D. M. W. Frierson, and D. L. Hartmann, 2012: Southern Hemisphere jet latitude biases in CMIP5 models linked to shortwave cloud forcing. *Geophys. Res. Lett.*, **39**, L19708, doi:10.1029/2012GL053115.

——, M. D. Zelinka, and D. L. Hartmann, 2014: The response of the Southern Hemispheric eddy-driven jet to future changes in shortwave radiation in CMIP5. *Geophys. Res. Lett.*, **41**, 3244–3250, doi:10.1002/2014GL060043.

——, D. L. Hartmann, and M. J. Webb, 2016a: Mechanisms of the negative shortwave cloud feedback in middle to high latitudes. *J. Climate*, **29**, 139–157, doi:10.1175/JCLI-D-15-0327.1.

——, D. T. McCoy, and D. L. Hartmann, 2016b: Observational evidence for a negative shortwave cloud feedback in middle to high latitudes. *Geophys. Res. Lett.*, **43**, 1331–1339, doi:10.1002/2015GL067499.

Cess, R. D., and Coauthors, 1990: Intercomparison and interpretation of climate feedback processes in 19 atmospheric general circulation models. *J. Geophys. Res.*, **95**, 16 601–16 615, doi:10.1029/JD095iD10p16601.

Chen, G., R. A. Plumb, and J. Lu, 2010: Sensitivities of zonal mean atmospheric circulation to SST warming in an aqua-planet model. *Geophys. Res. Lett.*, **37**, L12701, doi:10.1029/2010GL043473.

Colman, R., 2003: A comparison of climate feedbacks in general circulation models. *Climate Dyn.*, **20**, 865–873, doi:10.1007/s00382-003-0310-z.

——, and B. J. McAvaney, 1997: A study of general circulation model climate feedbacks determined from perturbed sea surface temperature experiments. *J. Geophys. Res.*, **102**, 19 383–19 402, doi:10.1029/97JD00206.

Dal Gesso, S., J. J. van der Dussen, A. P. Siebesma, S. R. de Roode, I. A. Boutle, Y. Kamae, R. Roehrig, and J. Vial, 2015: A single-column model intercomparison on the stratocumulus representation in present-day and future climate. *J. Adv. Model. Earth Syst.*, **7**, 617–647, doi:10.1002/2014MS000377.

Delcambre, S. C., D. J. Lorenz, D. J. Vimont, and J. E. Martin, 2013: Diagnosing Northern Hemisphere jet portrayal in 17 CMIP3 global climate models: Twenty-first-century projections. *J. Climate*, **26**, 4930–4946, doi:10.1175/JCLI-D-12-00359.1.

Deser, C., R. A. Tomas, and L. Sun, 2015: The role of ocean–atmosphere coupling in the zonal-mean atmospheric response to Arctic sea ice loss. *J. Climate*, **28**, 2168–2186, doi:10.1175/JCLI-D-14-00325.1.

Frierson, D. M. W., J. Lu, and G. Chen, 2007: Width of the Hadley cell in simple and comprehensive general circulation models. *Geophys. Res. Lett.*, **34**, L18804, doi:10.1029/2007GL031115.

Gordon, N. D., and S. A. Klein, 2014: Low-cloud optical depth feedback in climate models. *J. Geophys. Res.*, **119**, 6052–6065, doi:10.1002/2013JD021052.

Graversen, R. G., and M. Wang, 2009: Polar amplification in a coupled climate model with locked albedo. *Climate Dyn.*, **33**, 629–643, doi:10.1007/s00382-009-0535-6.

Gregory, J., and M. Webb, 2008: Tropospheric adjustment induces a cloud component in CO_2 forcing. *J. Climate*, **21**, 58–71, doi:10.1175/2007JCLI1834.1.

Grise, K. M., and B. Medeiros, 2016: Understanding the varied influence of midlatitude jet position on clouds and cloud radiative effects in observations and global climate models. *J. Climate*, **29**, 9005–9025, doi:10.1175/JCLI-D-16-0295.1.

——, and L. M. Polvani, 2016: Is climate sensitivity related to dynamical sensitivity? *J. Geophys. Res.*, **121**, 5159–5176, doi:10.1002/2015JD024687.

——, ——, G. Tselioudis, Y. Wu, and M. D. Zelinka, 2013: The ozone hole indirect effect: Cloud-radiative anomalies accompanying the poleward shift of the eddy-driven jet in the Southern Hemisphere. *Geophys. Res. Lett.*, **40**, 3688–3692, doi:10.1002/grl.50675.

Hall, A., and S. Manabe, 1999: The role of water vapor feedback in unperturbed climate variability and global warming. *J. Climate*, **12**, 2327–2346, doi:10.1175/1520-0442(1999)012<2327:TROWVF>2.0.CO;2.

——, and X. Qu, 2006: Using the current seasonal cycle to constrain snow albedo feedback in future climate change. *Geophys. Res. Lett.*, **33**, L03502, doi:10.1029/2005GL025127.

Hansen, J., M. Sato, and R. Ruedy, 1997: Radiative forcing and climate response. *J. Geophys. Res.*, **102**, 6831–6864, doi:10.1029/96JD03436.

Hartmann, D. L., and K. Larson, 2002: An important constraint on tropical cloud–climate feedback. *Geophys. Res. Lett.*, **29**, 1951, doi:10.1029/2002GL015835.

Harvey, B. J., L. C. Shaffrey, and T. J. Woollings, 2014: Equator-to-pole temperature differences and the extra-tropical storm track responses of the CMIP5 climate models. *Climate Dyn.*, **43**, 1171–1182, doi:10.1007/s00382-013-1883-9.

Hawcroft, M., H. Dacre, R. Forbes, K. Hodges, L. Shaffrey, and T. Stein, 2017: Using satellite and reanalysis data to evaluate the representation of latent heating in extratropical cyclones in a climate model. *Climate Dyn.*, **48**, 2255–2278, doi:10.1007/s00382-016-3204-6.

Held, I. M., and B. J. Soden, 2000: Water vapor feedback and global warming. *Annu. Rev. Energy Environ.*, **25**, 441–475, doi:10.1146/annurev.energy.25.1.441.

——, and K. M. Shell, 2012: Using relative humidity as a state variable in climate feedback analysis. *J. Climate*, **25**, 2578–2582, doi:10.1175/JCLI-D-11-00721.1.

Ingram, W., 2010: A very simple model for the water vapour feedback on climate change. *Quart. J. Roy. Meteor. Soc.*, **136**, 30–40, doi:10.1002/qj.546.

——, 2013: A new way of quantifying GCM water vapour feedback. *Climate Dyn.*, **40**, 913–924, doi:10.1007/s00382-012-1294-3.

Kay, J. E., B. Medeiros, Y.-T. Hwang, A. Gettelman, J. Perket, and M. G. Flanner, 2014: Processes controlling Southern Ocean

shortwave climate feedbacks in CESM. *Geophys. Res. Lett.*, **41**, 616–622, doi:10.1002/2013GL058315.

——, C. Wall, V. Yettella, B. Medeiros, C. Hannay, P. Caldwell, and C. Bitz, 2016: Global climate impacts of fixing the Southern Ocean shortwave radiation bias in the Community Earth System Model (CESM). *J. Climate*, **29**, 4617–4636, doi:10.1175/JCLI-D-15-0358.1.

Kidston, J., S. M. Dean, J. A. Renwick, and G. K. Vallis, 2010: A robust increase in the eddy length scale in the simulation of future climates. *Geophys. Res. Lett.*, **37**, L03806, doi:10.1029/2009GL041615.

Klein, S. A., and A. Hall, 2015: Emergent constraints for cloud feedbacks. *Curr. Climate Change Rep.*, **1**, 276–287, doi:10.1007/s40641-015-0027-1.

Kushner, P. J., I. M. Held, and T. L. Delworth, 2001: Southern Hemisphere atmospheric circulation response to global warming. *J. Climate*, **14**, 2238–2249, doi:10.1175/1520-0442(2001)014<0001:SHACRT>2.0.CO;2.

Mauritsen, T., R. G. Graversen, D. Klocke, P. L. Langen, B. Stevens, and L. Tomassini, 2013: Climate feedback efficiency and synergy. *Climate Dyn.*, **41**, 2539–2554, doi:10.1007/s00382-013-1808-7.

McCoy, D. T., D. L. Hartmann, M. D. Zelinka, P. Ceppi, and D. P. Grosvenor, 2015: Mixed-phase cloud physics and Southern Ocean cloud feedback in climate models. *J. Geophys. Res. Atmos.*, **120**, 9539–9554, doi:10.1002/2015JD023603.

——, R. Eastman, D. L. Hartmann, and R. Wood, 2017: The change in low cloud cover in a warmed climate inferred from AIRS, MODIS, and ECMWF-Interim. *J. Climate*, **30**, 3609–3620, doi:10.1175/JCLI-D-15-0734.1.

Medeiros, B., D. L. Williamson, and J. G. Olson, 2016: Reference aquaplanet climate in the Community Atmosphere Model, version 5. *J. Adv. Model. Earth Syst.*, **8**, 406–424, doi:10.1002/2015MS000593.

Neale, R. B., and Coauthors, 2010: Description of the NCAR Community Atmosphere Model (CAM 4.0). NCAR Tech. Note TN-485, 212 pp.

Neggers, R. A. J., 2015: Attributing the behavior of low-level clouds in large-scale models to subgrid-scale parameterizations. *J. Adv. Model. Earth Syst.*, **7**, 2029–2043, doi:10.1002/2015MS000503.

Pithan, F., and T. Mauritsen, 2014: Arctic amplification dominated by temperature feedbacks in contemporary climate models. *Nat. Geosci.*, **7**, 181–184, doi:10.1038/ngeo2071.

Previdi, M., and B. G. Liepert, 2012: The vertical distribution of climate forcings and feedbacks from the surface to top of atmosphere. *Climate Dyn.*, **39**, 941–951, doi:10.1007/s00382-011-1233-8.

Qu, X., and A. Hall, 2014: On the persistent spread in snow-albedo feedback. *Climate Dyn.*, **42**, 69–81, doi:10.1007/s00382-013-1774-0.

——, ——, S. A. Klein, and P. M. Caldwell, 2014: On the spread of changes in marine low cloud cover in climate model simulations of the 21st century. *Climate Dyn.*, **42**, 2603–2626, doi:10.1007/s00382-013-1945-z.

——, ——, ——, and A. M. DeAngelis, 2015: Positive tropical marine low-cloud cover feedback inferred from cloud-controlling factors. *Geophys. Res. Lett.*, **42**, 7767–7775, doi:10.1002/2015GL065627.

Rieck, M., L. Nuijens, and B. Stevens, 2012: Marine boundary layer cloud feedbacks in a constant relative humidity atmosphere. *J. Atmos. Sci.*, **69**, 2538–2550, doi:10.1175/JAS-D-11-0203.1.

Ring, M. J., and R. A. Plumb, 2008: The response of a simplified GCM to axisymmetric forcings: Applicability of the fluctuation–dissipation theorem. *J. Atmos. Sci.*, **65**, 3880–3898, doi:10.1175/2008JAS2773.1.

Roe, G. H., N. Feldl, K. C. Armour, Y.-T. Hwang, and D. M. W. Frierson, 2015: The remote impacts of climate feedbacks on regional climate predictability. *Nat. Geosci.*, **8**, 135–139, doi:10.1038/ngeo2346.

Schneider, E. K., B. P. Kirtman, and R. S. Lindzen, 1999: Tropospheric water vapor and climate sensitivity. *J. Atmos. Sci.*, **56**, 1649–1658, doi:10.1175/1520-0469(1999)056<1649:TWVACS>2.0.CO;2.

Shepherd, T. G., 2014: Atmospheric circulation as a source of uncertainty in climate change projections. *Nat. Geosci.*, **7**, 703–708, doi:10.1038/ngeo2253.

Sherwood, S. C., S. Bony, and J.-L. Dufresne, 2014: Spread in model climate sensitivity traced to atmospheric convective mixing. *Nature*, **505**, 37–42, doi:10.1038/nature12829.

Sigmond, M., and J. F. Scinocca, 2010: The influence of the basic state on the Northern Hemisphere circulation response to climate change. *J. Climate*, **23**, 1434–1446, doi:10.1175/2009JCLI3167.1.

Simpson, I. R., and L. M. Polvani, 2016: Revisiting the relationship between jet position, forced response and annular mode variability in the southern midlatitudes. *Geophys. Res. Lett.*, **43**, 2896–2903, doi:10.1002/2016GL067989.

——, R. Seager, M. Ting, and T. A. Shaw, 2015: Causes of change in Northern Hemisphere winter meridional winds and regional hydroclimate. *Nat. Climate Change*, **6**, 65–70, doi:10.1038/nclimate2783.

Soden, B. J., I. M. Held, R. Colman, K. M. Shell, J. T. Kiehl, and C. A. Shields, 2008: Quantifying climate feedbacks using radiative kernels. *J. Climate*, **21**, 3504–3520, doi:10.1175/2007JCLI2110.1.

Stevens, B., and S. Bony, 2013: What are climate models missing? *Science*, **340**, 1053–1054, doi:10.1126/science.1237554.

——, and Coauthors, 2013: Atmospheric component of the MPI-M Earth System Model: ECHAM6. *J. Adv. Model. Earth Syst.*, **5**, 146–172, doi:10.1002/jame.20015.

Taylor, K. E., R. J. Stouffer, and G. A. Meehl, 2012: An overview of CMIP5 and the experiment design. *Bull. Amer. Meteor. Soc.*, **93**, 485–498, doi:10.1175/BAMS-D-11-00094.1.

Tomas, R. A., C. Deser, and L. Sun, 2016: The role of ocean heat transport in the global climate response to projected Arctic sea ice loss. *J. Climate*, **29**, 6841–6859, doi:10.1175/JCLI-D-15-0651.1.

Tsushima, Y., and Coauthors, 2006: Importance of the mixed-phase cloud distribution in the control climate for assessing the response of clouds to carbon dioxide increase: A multimodel study. *Climate Dyn.*, **27**, 113–126, doi:10.1007/s00382-006-0127-7.

Vial, J., J.-L. Dufresne, and S. Bony, 2013: On the interpretation of inter-model spread in CMIP5 climate sensitivity estimates. *Climate Dyn.*, **41**, 3339–3362, doi:10.1007/s00382-013-1725-9.

Voigt, A., and T. A. Shaw, 2015: Circulation response to warming shaped by radiative changes of clouds and water vapour. *Nat. Geosci.*, **8**, 102–106, doi:10.1038/ngeo2345.

——, and ——, 2016: Impact of regional atmospheric cloud radiative changes on shifts of the extratropical jet stream in response to global warming. *J. Climate*, **29**, 8399–8421, doi:10.1175/JCLI-D-16-0140.1.

Wall, C. J., and D. L. Hartmann, 2015: On the influence of poleward jet shift on shortwave cloud feedback in global climate

models. *J. Adv. Model. Earth Syst.*, **7**, 2044–2059, doi:10.1002/2015MS000520.

Wetherald, R. T., and S. Manabe, 1988: Cloud feedback processes in a general circulation model. *J. Atmos. Sci.*, **45**, 1397–1416, doi:10.1175/1520-0469(1988)045<1397:CFPIAG>2.0.CO;2.

Yin, J. H., 2005: A consistent poleward shift of the storm tracks in simulations of 21st century climate. *Geophys. Res. Lett.*, **32**, L18701, doi:10.1029/2005GL023684.

Zappa, G., and T. G. Shepherd, 2017: Storylines of atmospheric circulation change for European regional climate impact assessment. *J. Climate*, **30**, 6561–6577, doi:10.1175/JCLI-D-16-0807.1.

——, B. J. Hoskins, and T. G. Shepherd, 2015: Improving climate change detection through optimal seasonal averaging: The case of the North Atlantic jet and European precipitation. *J. Climate*, **28**, 6381–6397, doi:10.1175/JCLI-D-14-00823.1.

Zelinka, M. D., and D. L. Hartmann, 2010: Why is longwave cloud feedback positive? *J. Geophys. Res.*, **115**, D16117, doi:10.1029/2010JD013817.

——, S. A. Klein, and D. L. Hartmann, 2012: Computing and partitioning cloud feedbacks using cloud property histograms. Part II: Attribution to changes in cloud amount, altitude, and optical depth. *J. Climate*, **25**, 3736–3754, doi:10.1175/JCLI-D-11-00249.1.